TÉCNICO LISBOA

Characterization of acid solids by proton/deuterium exchange followed by infrared spectroscopy

Catarina Simão Marta

Thesis to obtain the Master of Science Degree in

Chemical Engineering

Supervisor: Doctor Mickaël Rivallan

Supervisor: Professor Carlos Manuel Faria de Barros Henriques

Examination Committee

Chairperson: Professor Mário Nuno de Matos Sequeira Berberan e Santos

Supervisor: Professor Carlos Manuel Faria de Barros Henriques

Member of the Committee: Professor José Manuel Félix Madeira Lopes

October 2019

Declaration

I declare that this document is an original work of my own authorship and that it fulfills all the requirements of the Code of Conduct and Good Practices of the Universidade de Lisboa.

Acknowledgments

I would like to reserve this section to sincerely thank all of those that contributed to this report.

First and foremost, I am truly grateful for the guidance provided by my supervisors, Dr. Mickaël Rivallan, Dr. Anne-Claire Dubreuil and Dr. Arnold Lambert during the six months I stayed at IFPEN. I cannot forget to mention Dr. Gerhard Pirnbruger for the interest shown towards my work, as well as technicians Emmanuel Soyer and Isabel Clémencon for all the help they have provided me in the lab and for so kindly welcoming me into IFPEN.

I would also like to thank my supervisor at IST, Prof. Dr. Carlos Henriques, for always being available and for the supervision provided during the course of my work.

Additionally, I would like to thank everyone at IST and IFPEN with whom I may have not closely interacted but who made my internship possible.

And last, but certainly not least, I would like to thank my family and my closest friends for always supporting me and keeping me motivated.

(This page was intentionally left in blank)

Resumo

O presente relatório descreve o desenvolvimento de uma técnica de caracterização baseada em espectroscopia de infravermelho, capaz de descrever precisamente a acidez superficial de zeólitos, cujas propriedades superficiais são de extrema importância para a sua aplicação eficiente como catalisadores.

Esta metodologia é baseada na utilização de benzeno deuterado (C_6D_6) como molécula sonda, formando deuteroxilos (OD) a partir de hidroxilos (OH) que se comportam como centros ácidos de Brønsted, ativos cataliticamente. A troca H/D é seguida por tempos de contacto entre C_6D_6 e amostra sucessivamente maiores.

Zéolitos com diferentes rácios de Si/Al e submetidos a diferentes tratamentos térmicos foram utilizados para validar esta metodologia. Os resultados mostraram que esta técnica é capaz de caracterizar simultaneamente grande parte dos centros ácidos, fornecendo informação quanto à sua acessibilidade e força ácida. Adicionalmente, é suficientemente sensível à influência de parâmetros distintos, tais como a distribuição de centros ácidos de acordo com o rácio Si/Al, e a modificação da acidez provocada por diferentes tratamentos. Os resultados foram obtidos numa região de números de onda que apenas contém os grupos hidroxilo permutados, fornecendo informação muito mais detalhada quanto à distribuição e quantificação dos centros ácidos em comparação com outras moléculas sonda e métodos de caracterização.

Palavras-chave: zeólito Y, permuta H/D, infravermelho, espectroscopia, caracterização, benzeno deuterado

(This page was intentionally left in blank)

Abstract

The present report concerns the development of an infrared spectroscopy characterization technique capable of precisely describing the surface acidity of zeolites, whose surface properties comprehension is of key importance for their efficient application as catalysts.

This methodology is based on the use of perdeuterated benzene (C_6D_6) as a probe molecule, forming deuteroxyl groups (OD) at the expense of hydroxyl groups (OH) which behave as Brønsted acid sites, catalytically active. The H/D exchange is followed according to the increasing time contacts of the sample with C_6D_6.

Faujasite zeolites with different Si/Al ratios and subjected to different thermal treatments were used to validate this methodology. The results have shown that this technique is capable of simultaneously characterizing most of the acid sites found on zeolites, screening their accessibility and their acidic strength. Additionally, it is sensitive enough to study the influence of distinct parameters, such as the distribution of acid sites according to the Si/Al ratio, and the alteration of the acidity by modification treatments. The results were obtained on a wavenumber range which only contains the hydroxyl groups that have undergone H/D exchange, providing more detailed information on the distribution and quantification of the acid sites when compared to other probe molecules and characterization techniques.

Keywords: zeolite Y, H/D exchange, infrared, spectroscopy, characterization, perdeuterobenzene

(This page was intentionally left in blank)

Table of Contents

List of Figures

List of Tables

(This page was intentionally left in blank)

Nomenclature

AlPO	Aluminophosphate
ASA	Amorphous Silica Alumina
BAS	Brønsted Acid Sites
C_6D_6	Perdeuterated benzene
DTGS	Deuterated Triglycine Sulphate
FT-IR	Fourier Transform Infrared
H/D	Proton/ deuterium
IR	Infrared
IRMS	Infrared Mass Spectroscopy
LAS	Lewis Acid Sites
LPG	Liquid Petroleum Gas
MAS	Magic Angle Spinning
MCT	Mercury-Cadmium-Tellurium
MeAPO	Metal Aluminophosphate
MOF	Metal Organic Framework
MR	Member Ring
NMR	Nuclear Magnetic Resonance
NO_x	Nitrogen oxides
OD	Deuteroxyl
OH	Hydroxyl
SAPO	Silicoaluminophosphate
SCR	Selective Catalytic Reduction
Si/Al	Silicon to aluminum ratio
TPD	Temperature Programmed Desorption
USY	Ultra Stable Y
VGO	Vacuum Gas Oil
VOC	Volatile Organic Compounds
XPS	X-ray Photoelectron Spectroscopy
v(OH)	Hydroxyl stretching vibration

(This page was intentionally left in blank)

1 Introduction

1.1 Relevance of the subject

It is thanks to catalysis that a large number of reactions and industrial processes can be carried out at operating conditions that make them economically feasible, and there is no shortage of examples that illustrate its importance and contribution to the currently employed industrial processes. For instance, the synthesis of ammonia by the Haber-Bosch process (1909) was the first process carried out on a large-scale, providing an extreme reduction of the severity of operating conditions needed to obtain this compound. Other processes worth mentioning are the Fischer-Tropsch process to convert synthesis gas to motor fuels (1923) and the catalytic cracking of oil (1936) [1].

By employing catalysts, catalytically unfavored reactions can be performed under relatively mild operating conditions and, to this day, catalysis is, undoubtedly, the essence behind most of the current petroleum-based processes, namely those performed in oil refineries. Oil became the paramount source of transportation fuels and chemicals after World War II and was the feedstock from which higher value products such as liquid petroleum gas (LPG), gasoline, kerosene, jet fuel, diesel fuel, lubricants and other petrochemicals could be obtained [1].

Since then, catalysis has been intimately related to society's ever-growing energy demands and fuel consumption. These have, in turn, triggered the emergence of increasingly complex and urgent environmental concerns, leading to the development of new fields and applications for catalysis, namely the extensive work performed on Selective Catalytic Reduction (SCR) catalysts to limit the environmental emissions of nitrogen oxides (NO_x) produced by the combustion of fossil fuels [2–5] or the catalytic conversion of volatile organic compounds (VOCs) [6].

There is currently an exhaustive number of catalysts reported in the literature used for a variety of applications, and this number is expected to continue to steadily grow. Among these, zeolites may be the most prominent and used catalysts, as a result of their molecular sieving, shape selectivity and ion exchanging properties [6].

The acidity and porosity that these materials possess are at the base of their application in catalytic processes, so in order to synthesize more acidic and selective catalysts, a better understanding of their properties is of paramount importance. This can be obtained by a thorough characterization of the active sites, regarding their nature (Brønsted or Lewis acid sites), number, strength and strength distribution. A typical question resides in correlating these characteristics with their catalytic performance.

Nevertheless, despite the humongous amount of literature found on these topics, a lot is still undisclosed and the role of acidity remains not fully understood [7]. Thus, the aim of the present report is to develop a technique capable of contributing to the comprehension of the acidity role in these materials, by employing infrared spectroscopy, a popular technique that has been used since the

1960s for the characterization of acid solids portraying catalytic activity, usually being coupled with *in situ* adsorption studies using probe molecules. In this report, it is intended to study how perdeuterobenzene (C_6D_6) performs on a set of faujasite Y and USY zeolites. By employing this probe molecule, the distinction of the acid sites will be obtained on a region of the spectrum containing information solely on the hydroxyl groups which have undergone H/D exchange, thus providing a more accurate distribution and quantification when compared to other probe molecules and characterization techniques.

1.2 Scope of the report

The present report comprises a Bibliographic Study, introducing relevant concepts. Afterwards, the experimental setup and procedure that have been employed will be presented in the Experimental Part.

The data treatment strategy will be included in chapter 4, entitled Problems and Difficulties. Posteriorly, the results will be presented and discussed according to each different effect under study. Additionally, the technique will be compared to the results obtained when using pyridine as probe molecule.

Final conclusions on the technique will be presented, as well as perspectives for future works, where results using different probe molecules will also be disclosed.

2 Bibliographic Study

2.1 Catalysis and catalysts

Catalysis has undergone extensive research throughout the years, and it is present in at least one step of most current industrial processes. The term was first coined by Berzelius, who observed that certain substances could trigger decomposition and synthesis reactions just by their presence, due to what he then called their “catalytic strength”. It was only with the work performed by Ostwald (1895) that the current definition of a catalyst was created, i.e. a substance capable of altering the speed of a reaction without being consumed in the process [6].

Since then, major contributions have led to the exponential growth and comprehension gathered in this field of studies, such as the findings in the 1920’s concerning unstable intermediate compounds by Sabatier, or the contributions made by the Langmuir equation and the BET isotherm during the 1940’s, respectively in the description of the chemical adsorption equilibria (introduced by Van’t Hoff) and the determination of the specific surface area of catalysts [6].

The next decades were marked by extensive progress on experimental techniques such as infrared spectroscopy during the 1950’s and by the introduction of the first synthetic zeolites, triggering profound modifications in refining and petroleum-based processes up to this day. The shape selectivity concept of catalysts was also introduced around this time by Wiesz [8,9].

Other contributions followed during the 1970’s and the 1980’s, based on the development of new techniques capable of shedding light on the catalytic processes on an atomic scale and on a better preparation of catalysts. New types of porous materials for catalysis applications have also been synthesized, such as zeotypes (SAPOs, AlPOs and MeAPOs) [6], and new fields of application have emerged, namely environmental, photo- or electrocatalysis.

Catalytic processes are carried out by employing catalysts. The introduction of a catalyst provides a new reaction pathway, more energetically favorable than the original route, as it reduces the energy of activation, accelerating the reaction. Ideally, as catalysts are not consumed in the reaction, they could be repeatedly employed without loss of properties but, in reality, they suffer progressive deactivation in each cycle they participate in.

The life expectancy of a catalyst is intrinsically related to its characteristics and, as a result, to the characteristics of the process in which it will be employed, namely the severity of the operating conditions. For instance, cracking catalysts have a very short life expectancy, in opposition to those used in ammonia synthesis [6].

Catalysts can be exclusively made of the active phase, or supported, i.e. the active phase is dispersed on a refractory support material. Catalytic agents, often metals or metal oxides, or promoters (species without catalytic activity but which improve the activity and/or the selectivity of the catalyst) can be considered active substances. The most used support is alumina (Al_2O_3), but silica (SiO_2), aluminosilicates and other carbon materials can also be employed.

The activity, selectivity, mechanical strength, stability and thermal conductivity of a catalyst is intimately related to its composition and preparation procedure. Diffusion limitations, either internal or external, can further modify its acidity, so preventive measures should be taken.

There are currently a broad number of porous solids containing acid sites. Among these, the most commonly employed are aluminosilicates such as zeolites, clays and amorphous silica alumina (ASA), but other types of solids can be applied as well, such as magnesium, zinc and cerium oxides, along with alumina and silica, to name a few [6,10]. Other types of acid solids, such as metal organic frameworks (MOF), have also gained quite a lot of popularity in recent years [6].

2.1.1 Zeolite Y

The majority of the produced zeolites is employed in the manufacture of detergents, substituting water softeners such as tripolyphosphates which cause eutrophication of lakes and rivers [6]. In addition, these solids play a crucial role in catalytic processes carried out in refineries and petrochemistry, as well as in organic synthesis and depollution applications. Main applications of these acid solids include ion exchange, adsorption, and catalysis.

Zeolites are one of the most important classes of catalysts. The term translates from the Greek to “boiling stone” and alludes to their bubbling properties when heated at high temperatures. These are very porous aluminosilicates, with a structure composed by submicroscopic interconnected channels [11]. The boiling properties observed in these materials are related to the water adsorption taking place in these channels, easily removed by heating up the material, without inflicting any damage to the structure [12].

Zeolites are porous aluminosilicates with a tridimensional structure formed by TO_4 tetrahedra (SiO_4 or AlO_4^- , as T=Si or Al atoms) linked together by oxygen atoms [6,13,14]. These, in turn, originate the unit cells, described by expression *(2.1.1.1)* [6], where n relates to the valence of the cation M, x and y are the total number of tetrahedra by unit cell and y/x is equivalent to the atomic Si/Al ratio. This ratio can oscillate between 1, as by the Loewenstein’s rule, no Al tetrahedra can be linked to a neighboring Al tetrahedral (Al-O-Al groups are too unstable), and infinite [6]. The T-O-T (inter-tetrahedrons) angle can vary between 130º and 180º, giving rise to many zeolite structures [6,9]. As the angle increases, the strength of the T-O bond increases, whereas the strength of the O-H bond decreases, thus resulting in higher acidity [15].

$$M_{x/y}^{n+}(AlO_2^-)_x(SiO_2)_y \qquad (2.1.1.1)$$

Silicon tetrahedra are neutrally charged, as the positive charges in Si^{4+} are balanced by each of the oxygen anions to which it is bound. Aluminum tetrahedra display a negative charge, as a result of aluminum in its Al^{3+} ionic form being shared by four oxygen anions, each with a negative charge. This positive charge deficit doesn’t counterbalance one of the oxygen anions, being the reason for the overall negative charge of zeolites [10]. In order to achieve electroneutrality, these negative charges

need to be balanced out by compensation cations, usually sodium (Na^+) or other alkaline or alkaline earth metals.

As ion exchange can be easily performed on zeolites, these metal cations can be exchanged with other ions, namely ammonium and quaternary ammonium [12] but the most interesting is when these are replaced by protons, giving rise to acidic zeolites. These protons attached to the framework oxygen atoms constitute Brønsted acid sites (BAS), responsible for the catalytic activity of zeolites [13].

Aside from these acid sites, other types can be found on zeolites, namely Lewis acid sites (LAS), basic sites and redox centers, making them suitable for applications in acid, basic, acid-base, redox and bi-functional catalysis [6].

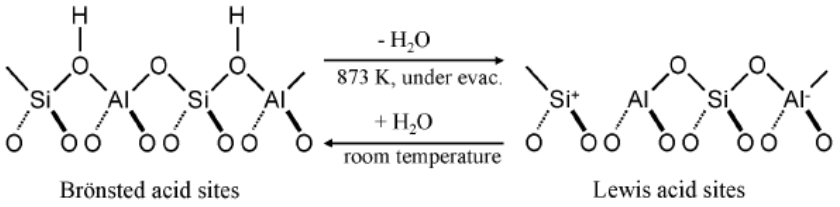

Figure 1 : Brønsted and Lewis acid sites in catalysts. Taken from [16]

Direct exchange of the sodium form of a zeolite into its protonic form is not advisable, as acids like hydrochloric acid employed in these treatments tend to attack and damage the silica-alumina network. Instead, this exchange is performed in an indirect manner, by first exchanging the sodium ions with ammonium ions, resulting in a zeolite in its ammonium form [6]. The protonic form is easily obtained by heating the resulting zeolite to a few hundred degrees (calcination), thus enabling the decomposition of the ammonium anions into gaseous ammonia, leaving behind a proton [17,18].

Zeolites contain pores of molecular dimensions, making them compatible with a huge number of molecules of industrial interest. These pores can be considered molecular reactors or nanoreactors. The shape and dimensions of these pores influence the selectivity, speed and stability of the reactions, as do the properties of the acid sites. Thus, they show shape selectivity, which can be related to the products, the reactants, the transition state and can explain the constraint effect in the micropores [19].

The pore sizes of zeolites can range from 3–12 Å to 0.5–1.2 nm [6,12,13]. Depending on these dimensions and on the type of structure, they can act as molecular sieves, being able to separate different molecules according to their shape and dimensions.

Zeolite structures consist in n T atoms linked in a ring by O ions atoms, which create the so called n membered rings (n-MR), of 8-MR for small pore zeolites (3-5 Å), 10-MR for zeolites with intermediate pores (5–6.5 Å), and 12-MR or higher for large pore zeolites (6.5 to 8 Å). The latter two are the most relevant for catalysis, as they may combine high conversion with shape selectivity features.

Depending on the pore size diameter, zeolites can display micro-, meso- or macroporosity, or a combination thereof. The porous framework can be defined as uni-, bi- or tridimensional, containing channels that may or may not be interconnected. The unique porous structure in each zeolite accounts for their shape selectivity and for the rates and modes of diffusion of different molecules. Preferential diffusion paths may exist depending on the relative sizes of the reactants and products [13]. This is the concept behind the molecular sieving properties found in zeolites, which can work both for reactants and as a mean to screen the type of products that result from a certain reaction.

The compensation cation can be easily removed by ion exchange, another interesting characteristic of zeolites. This can be performed during synthesis or by post synthesis treatments and allows the creation of zeolites with a common structure but very different compositions. On a similar note, altering the type and distribution of the acid sites will modify the distribution of the compensating cation, as well as the surface properties of the zeolite.

Thus, it is possible to control the catalytic properties of the zeolites in order to improve their activity and selectivity, making them particularly attractive for refinery processes. In fact, zeolites have shown an increase of about 10.000 in activity, when compared to conventional catalysts [11], as well as a very long life time, especially concerning Y zeolite.

Zeolite can be formed naturally in alkaline environments with volcanic activity (with 40 different known types), but most of the zeolites employed in industrial processes are artificially synthesized, with more than 200 types presently identified [20]. The first synthetically prepared zeolite was coined zeolite A and made from Na, Si, and Al by Linde [12]. This zeolite is mainly used in adsorption and separation applications, due to its water adsorbing ability. Following zeolite A, zeolite X and Y were synthesized, and they have been extensively used in catalytic cracking processes since the early 1960s [12]. Both zeolites have a faujasite type structure, illustrated in Figure 2.

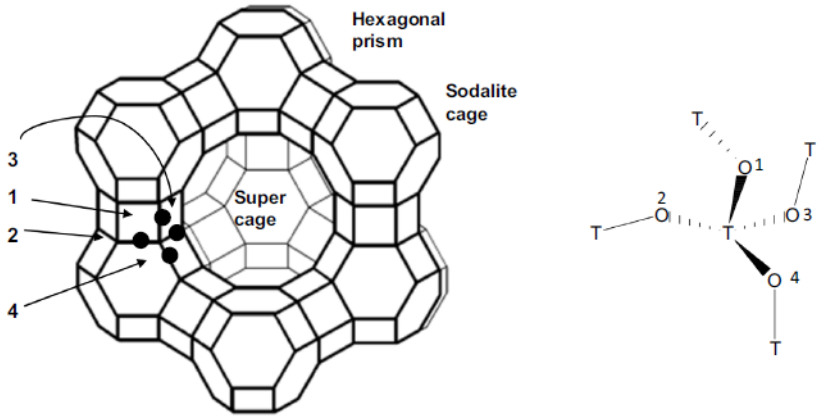

Figure 2 : Faujasite structure. Taken from [8]

Throughout time, the serious stability constraints found on zeolite X led to its replacement by zeolite Y, which was more hydrothermally stable due to its lower acidity (containing only 50% of the total acidity found in X zeolite [21]), and its higher SiO_2/Al_2O_3 ratio (Si/Al = 2.5). It should be mentioned

that zeolite Y has a major advantage over its X counterpart, as its Si/Al ratio can be increased and tuned using steam and/or acid treatments, while largely maintaining crystallinity.

Ultrastable Y (USY) zeolite appeared in the late 1970s and resulted from a framework dealuminated version of Y zeolite by calcination of its NH_4 form [18], followed by thermal treatment in the presence of steam under controlled temperatures.

Calcination directly influences several textural properties, such as the specific area, the porosity volume and the pore size distribution. Additionally, it can indirectly affect the activity, selectivity and stability of the catalyst. The main objective of this treatment is to create porosity while simultaneously increasing the mechanical strength of the catalyst. It is usually performed at high temperatures (higher than the reaction temperatures). The operating conditions during calcination, namely the gas flow (usually air or nitrogen), water presence, thickness of the catalyst bed, speed of heating and final temperature strongly influence the final properties of the catalyst [6].

Two different transformations can occur during calcination: one concerning the thermal decomposition of the active agents' precursors, the release of volatile substances and the formation of porosity, and the other related to the modification of the structure's crystalline/ amorphous profile.

Steaming is one of the many hydrothermal transformations that a catalyst can be subjected to, responsible for the stabilization of the structure and for making it more resistant to high temperatures [22,23]. By removing the aluminum content in the catalyst, the Si/Al ratio increases, and the overall acidity decreases. The dealumination of Y zeolites makes it possible to modulate the activity of the zeolite by controlling the Si/Al ratio of the framework and, therefore, the number of acid sites. The density of the acid sites decreases upon dealumination, in turn affecting the porosity, polarity (hydrophobicity) and reactivity.

On a similar note, mild steaming enhances the acidity and the reactivity [24]. As the steaming conditions get increasingly harsher, the accessibility of the sites increases due to the creation of mesopores. Nevertheless, severe dealumination might ensue, corresponding to a significant loss of acidity (and activity) [25].

Extra-framework cations resulting from dealumination can be characterized by their size, electric charge and chemical reactivity. All of these properties affect the cation siting and its coordination in the zeolite system and strongly define the exchange ability and catalytic potential of the zeolite [9].

Steam stabilized catalysts, like USY, are industrially popular as they are less prone to surface modifications [22], avoiding structure collapse, for instance. The Si/Al ratio is usually kept around 6 or higher in these catalysts, resulting in improved catalytic and hydrothermal stability.

Presently, Y and USY zeolites are used in various petrochemical applications, due to their remarkable activity and (shape) selectivity. Among different applications, USY zeolites are responsible for converting vacuum gas oil (VGO) into middle distillates, reducing the selectivity towards gasoline and gas, thus complying to the high diesel demands of the automobile industry [26].

This is obtained by employing bi-functional catalysts: they contain both acidic cracking and hydrogenation functions with the acidity being provided by (stabilized) faujasite zeolites and/or amorphous silica–alumina [19]. ASAs are mesoporous, so they are less prone to diffusion limitations even when dealing with bulky hydrocarbons, that very often occur in zeolites. Additionally, they exhibit moderate acidity (containing both Brønsted and Lewis acid sites), making them much more suitable than zeolites for the cracking of middle fractions. In fact, strong sites are often associated with a premature deactivation of the catalyst due to deposition of coke, leaving part of the acid sites inaccessible for the reacting species [1]. Thus, adding a zeolitic contribution to an ASA can improve the activity, while maintaining the selectivity towards middle distillates [27].

2.2 Brief introduction to infrared spectroscopy

Infrared spectroscopy has been crucial for collecting information about the acidic properties of catalysts, such as zeolites. Infrared (IR) light was discovery in 1800 by Herschel, and has been used in heterogeneous catalysis since the 1960's, with the publication of the first *in situ* studies dating back to the 1970's. This field of studies was during the 1980's revolutionized with the arrival of the first Fourier Transform Infrared (FT-IR) spectrometers which solved many of the issues related to conventional spectrometers [14].

Conventional spectrometers analyzed light by using a monochromator. Wavelengths would be sequentially analyzed, by dispersing light with the aid of a prism or a grid. FT-IR spectrometers, on the other hand, use an interferometer, which allows the simultaneous analysis of all wavelengths, considerably diminishing the time needed to obtain a spectrum in the whole range of frequencies [28]. The collected data in the interferogram allows the construction of a conventional looking spectrum by applying a Fourier transform, hence the name. Other advantages include the very low energy loss and the much higher signal to noise ratio obtained by digitally recording the spectrum.

An interferometer is composed by a beamsplitter and two mirrors, one fixed and the other moving. The light beam is divided in two before reaching the sample, being later recombined by the mirrors. The moving mirror creates a different path for half of the light beam, which will result in an interference. A sample spectrum will be collected by taking the difference between the instrument spectrum (background) and the spectrum of the instrument plus the sample.

Different beamspitters can be used, such as KBr for the mid-infrared, CaF_2 for the mid to near-infrared and CsI for the far-infrared region. Different types of IR sources can be employed, depending on the operating temperature and the desired spectral domain. Two different types of detectors can be used: thermal detectors called DTGS (deuterated triglycine sulphate) that measure the heat on a target, and more sensitive and precise detectors that count photons, defined as quantum detectors and known as MCT (mercury-cadmium-tellurium) [14].

IR radiation is arbitrarily divided in three regions: near (14000-4000 cm^{-1}), mid (4000-400 cm^{-1}) and far (400-10 cm^{-1}). The mid infrared is the most studied, as this interval comprises the vibronic

modes of typical groups. For instance, the stretching modes of zeolites hydroxyl groups (BAS) can be studied in this interval, with different wavenumbers corresponding to different types. These wavenumbers result from several factors: the chemical microenvironment (like the content and proximity of neighboring Al atoms), the coordination of the oxygen atom (terminal vs. bridged), geometric distribution of entities near the bond, like the zeolitic structure, and additional perturbations originated by exchangeable cations, extra-framework species or neighboring oxygen atoms [9,15]. Infrared spectroscopy can also provide information on the distortion of the T-O bond length or of the T-O-T or O-T-O angles by certain cations located in specific sites (by observing the bands appearing between 1000 and 850 cm^{-1}). The exact location will depend on the type of zeolite and substituting metal [9].

IR experiments can be performed in different modes (emission, diffuse reflectance, specular reflectance, etc [9,14,15]), but they are most often carried out in transmission mode, by measuring the transmittance, i.e. the ratio between the incident intensity read on the detector, I, and the incident intensity, I_o. Another definition for the transmittance is given by equation *(2.2.1)*, where ε_ν is the molar absorption coefficient (mol^{-1} dm^2 cm^{-1}) at a certain frequency ν and ce relates to the number of adsorbing species n (in mmol) per surface of the pellet (in cm^2), S, given by equation *(2.2.2)*.

$$T = \frac{I}{I_o} = e^{-\varepsilon_\nu ce} \qquad (2.2.1)$$

$$ce = \frac{n}{S} \qquad (2.2.2)$$

The transmittance can be easily converted to absorbance, d, by employing the Beer-Lambert equation *(2.2.3)*. By combining equations *(2.2.2)* and *(2.2.3)*, the final expression for the absorbance is given by equation *(2.2.4)*:

$$d = log_{10}\left(\frac{1}{T}\right) \qquad (2.2.3)$$

$$d = \varepsilon_\nu \left(\frac{n}{S}\right) \qquad (2.2.4)$$

Prior to the analysis, samples should undergo an activation procedure at high temperatures and under vacuum. Specifically concerning zeolites, this step aims at the removal of most of the adsorbed water (as up to 20% of a zeolite's mass can be due to moisture adsorption [9]) and impurities which might be present. A way of determining the degree of water removal is by observing its specific IR bands, namely the hydroxyl elongation vibration band at ~3500 cm^{-1} and its plane deformation at ~1600 cm^{-1}. The activation procedure should not be performed too fast, as it can trigger self-steaming on more sensitive zeolites, creating extra-framework aluminum species. Some of the most common impurities relate to carbonates, nitrates and sulphate, each easily identifiable by their respective IR bands [14].

Different bands can be attributed to the hydroxyl groups in the spectrum of a zeolite (see Table 1).

Table 1 : Attribution of different stretching OH vibrations on a Y zeolite [14]

Types of vibration	Wavenumber (cm^{-1})	Definition
Elongation, v(OH)	3785-3775	AlOH (Basic)
	3745	SiOH (Very weakly acidic)
	3680-3660	AlOH (Extra-framework species)
	3630	SiOHAl HFOH (Supercage)
	3610	SiOHAl HF'OH (Perturbed)
	3550	SiOHAl LFOH (Sodalite cage/hexagonal prism)
	3520	SiOHAl LF'OH (Perturbed)

A certain zeolite sample can contain surface hydroxyl groups of two kinds: stoichiometric OH groups which are represented in the chemical formula of a substance, and nonstoichiometric OH groups originated by defects in the crystal configurations (edge, corner or kink).

Stronger Brønsted sites (of higher acidity) can be found at lower wavenumbers [14,15]. A way of distinguishing between Brønsted sites in similar wavenumbers and of determining the presence of Lewis sites is by employing probe molecules. By following its adsorption, one can gather information on surface features, as well as the nature, strength, local arrangement and amount of different acids sites on the catalyst [9].

Probe molecules should be chosen according to the acid sites to be studied, Lewis or Brønsted. Lewis acid sites, LAS, are coordinatively unsaturated sites working as electron acceptors, and will bind to nucleophilic molecules. Brønsted acid sites, BAS, are proton donors, such as OH groups, and will form different complexes with basic molecules [14].

Appropriate probe molecules should meet certain requirements. They should be basic molecules with little acidic behavior and interact selectively to a certain type of acid sites while being sensitive to sites of different strength [9]. Probes should be stable on the surface, easily adsorbed on the solid, and not prone to hydrolysis or oxidation [6].

Smaller molecules are more interesting as these can access more constrained acid sites, opposed to bulkier molecules which are only sensitive to the external surface. The stoichiometry of the complex must be known, with 1:1 complexes being preferable [9]. Notwithstanding, both a smaller and a bulkier probe molecule can sometimes be used on the same sample, completing information on the strength and spatial distribution of the acid sites [15].

However, depending on the dimensions of both the probe molecule and the pores of the zeolites, a confinement effect can be exerted by the zeolitic structure on the probe molecule, which

may alter the properties of the probe and result in different adsorption behaviors by the same molecule in different microporous systems inside the same zeolite [15].

Some of the most commonly used probe molecules include pyridine, ammonia, carbon monoxide, nitriles and benzene. A vibrational mode can only absorb Infrared radiation if there is a change in the dipole moment of the molecule. This means that purely symmetrical molecules will not be visible in IR. However, molecules like ethylene can be used as probe molecules for IR because they lose their symmetry in the presence of BAS, as they may experience both localized interactions with balancing cations and non-specific dispersive interaction with the framework of oxygen atoms, allowing them to be used as probe molecules for IR [9].

Pyridine may be the most used probe molecule, due to its ease of usage and strong basicity that enables it to be protonated on strong BAS, to form hydrogen bonds with weak BAS (SiOH) or to be strongly coordinated on LAS, thus providing information on the nature and amount of the present acid sites. Pyridine forms three complexes on the surface of an oxide (see Figure 3), which can be observed between 1400 cm^{-1} and 1700 cm^{-1}: PyH^+ (pyridinium ion), PyL (coordinated to Lewis acid sites) and Py-HO (hydrogen bonding). Molar absorption coefficients, interesting in quantitative experiments to determine the number of acid sites per gram in a catalyst, can be found in the literature to be 1,3 cm μmol^{-1} and between 1,5 and 2 cm μmol^{-1}, respectively for PyH^+ (BAS at 1545 cm^{-1}) and PyL (LAS at 1450 cm^{-1}).

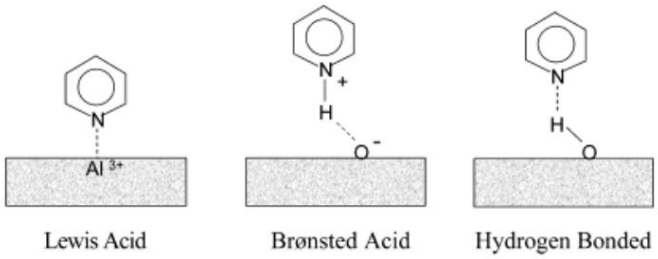

Figure 3 : Different pyridine complexes formed on a metal oxide surface. Taken from [29]

This molecule is stable up to high temperatures, enabling to study the acidity of zeolites in conditions closer to those of interesting reactions. However, some drawbacks should be addressed, namely steric hindrances related to its bigger dimensions and difficulties in properly cleaning up the setup after its introduction [9]. Another problem is related to the arbitrary choosing of the desorption temperature, which may strongly affect the results [1].

Carbon monoxide is a weak base extensively used due to its small dimensions. Despite not being protonated, it can perturb the proton by interaction with the carbon atom in the molecule. As the interaction with the acid sites is weak, the adsorption must be performed at low temperatures (usually at 100 K using liquid nitrogen). The vibration bands for BAS can be found between 2138 and 2170 cm^{-1} and around 2240 cm^{-1} for LAS [9,14]. The molar adsorption coefficient for BAS takes a typical value of 2,7 cm μmol^{-1} when using this probe molecule.

CO can be used to determine the coordination number in metal ions, as the interaction is much stronger in tetrahedral than in octahedral coordination like, for instance framework aluminum vs. extra-framework aluminum [9].

Nevertheless, this molecule also shows some drawbacks: for instance, there is some difficulty in discerning between signals corresponding to weak or to strong acid sites (specially with increasing aluminum content), coupled to difficult accurate quantification [1].

Ammonia is a very strong base whose small dimensions allow it to reach all the acid sites in a solid. It is very popular due to its high stability and ability to distinguish between BAS and LAS. Ammonia interacts with BAS by its free electron pair, but the stability of the adsorbed complex is strongly determined by the interaction of hydrogen atoms in ammonia with zeolite framework oxygens. The adsorption of this molecule is particularly complex, as it forms numerous adsorbed species interacting with both LAS and BAS. Moreover, this molecule can also interact with basic sites, thus displaying poor selectivity [30]. These problems are heightened when using aliphatic amines, as these portray higher acidity and, as a result, even lower selectivity. Significant quantitative results are difficult to obtain when using the aforementioned probe molecules.

Benzene is a weak base that interacts with protons via its π-electron cloud and can distinguish between acid sites with very close strength. However, the attribution to each of these sites might prove difficult and steric hindrances have been previously reported, preventing this molecule from reaching some of the acid sites contained in the samples [14].

Deuterated benzene has been increasingly used to study zeolites and other acid solids [31]. By contacting with a deuterated probe molecule, the sample undergoes H/D exchange, i.e. the hydroxyl groups (OH) are exchanged by deuteroxyl groups (OD). As the deuteron is heavier than the proton, the signal gets shifted to lower wavenumbers, the so called deuteroxyl region. The only contributions on this region will be the OD species that have been created, thus the acid sites that have been exchanged. This does not occur in the hydroxyl region, which comprises several signals attributed to non-acidic groups in addition to acid sites. Thus, by using deuterated benzene, not only is it possible to distinguish between acid sites of similar strength, but the quantification of each of these species is much more accurate.

2.3 Conventional characterization methods and their limitations

The catalytic activity of aqueous solutions can be predicted by the Hammett function, H_0, which employs a visual acidity scale built by using colored indicators, i.e. weak bases that can be easily converted to their conjugate acids by stronger acids. The H_0 acidity function can be given by equations *(2.3.1)* and *(2.3.2)*, where a_{H^+} is the activity of the proton and f_I and f_{HI^+} are, respectively, the activity coefficients of the indicator and of its conjugate acid. H_0 has a negative value for acids, with the most negative corresponding to the stronger acidity [15].

$$H_0 = -log(h_0) \qquad (2.3.1)$$

$$h_0 = \frac{a_{H^+} \cdot f_I}{f_{HI^+}} \qquad (2.3.2)$$

In aqueous solutions, the acid density or acid strength are often used as synonyms, as the universal acid responsible for proton transfer to a base is the hydroxonium cation H_3O^+ [6]. Thus, the extent of protonation depends mostly on the concentration of hydronium ions and not on the acid strength of the dissolved acid.

This is not the case when concerning acid solids, for which these are two very different concepts. The number and density of acid sites in acid solids is defined by chemical and structural parameters. As mentioned in the previous section, acid solids can contain Brønsted acid sites coexisting and interacting with Lewis acid sites, which makes the characterization of these materials much more complex [15].

Moreover, acid solids usually show an heterogenous surface, giving rise to a broad distribution of surface acid sites of distinct individual strength and density. This heterogeneity may be a consequence of partial neutralization of interacting sites, either by cation exchange, chemical reaction, dealumination and dehydroxylation procedures, or due to defects in the crystal framework [15]. In addition, confinement effects on microporous solids will strongly influence the accessibility of the sites. In this sense, acid sites on these solids cannot be characterized by a single number.

This method cannot differentiate between the acid strengths of various Brønsted acid sites found simultaneously on the surface of an acid solid, so other characterization methods have been developed to obtain this information. As both structural and chemical factors are involved, more than one characterization technique is often needed to obtain a valid correlation between acidity and catalytic activity [9]. The most reliable techniques will be disclosed below.

2.3.1 Adsorption-Desorption methods

A heterogenous catalyst undergoes a reaction cycle that can be divided in at least three steps: the adsorption of the reactants, followed by the activation and conversion of the active centers, finishing with the desorption of the products [9].

The acid strength of a site can be defined by the exchange of energy associated with the adsorption of a basic probe, or to desorb said molecule adsorbed state. The entropy of the probe molecule decreases upon adsorption, due to the reduction of its translational and rotational motion. So, in order to compensate for the decrease in entropy, adsorption is an exothermic process, with a corresponding energy release that can be measured either by adsorption microcalorimetry or by temperature programmed desorption (TPD). Both can provide information on the acid amount, the acid strength, and the distribution of acid sites, but the latter is run under more realistic operation conditions, thus providing more reliable information [9].

Several factors affect the results obtained by these techniques, such as the strength, number and type of acid sites, the zeolite structure, the probe's identity, and specific experimental conditions.

These techniques are attractive as they are relatively cheap, with an experimental procedure which can be easily modified, allowing its coupling with, for instance, *in situ* spectroscopic analysis, such as XPS-calorimetry or IR-TPD.

2.3.1.1 Adsorption microcalorimetry

Microcalorimetry measures the heat exchanged during adsorption of a certain probe on a clean surface. It consists in keeping the zeolite sample at a constant temperature in a sealed microcalorimeter [9], while pulses of probe molecule (usually pyridine or ammonia, but alkylamines are also interesting as they react selectively with BAS) are introduced at increasing vapor pressure to titrate the acid sites from highest to lowest strength [15]. The working temperature must be carefully chosen to minimize physisorption of the probe molecules and to fill all chemisorption sites. It should also be low enough (not higher than 600K) to minimize probe decomposition and to prevent its deposition at the pores' entrance, and high enough to reach adsorption-desorption equilibrium [9].

The resulting heat flow peaks are integrated, providing information on the number of adsorbed sites and on the heat of adsorption (the higher the heat of adsorption, the stronger is the acid site). A broad distribution of acid sites will be obtained due to the surface heterogeneity, which can be divided in three main contributions: the adsorption of LAS, which gives the highest values of heat of adsorption and the lowest coverage, while the adsorption of BAS will result in intermediate values of heat of adsorption. The lowest values of heat of adsorption and the highest coverage will be related to reversible adsorption or physisorption. Nevertheless, this technique may not be easily correlated with others, which is a significant drawback.

2.3.1.2 Temperature-programmed Desorption

Temperature-programmed desorption starts with the sample already saturated in probe molecule and is performed at a constant heating rate between an initial and a final temperature, following a temperature program [9,15]. The acquired heat flow curve gives information on the amount of desorbed species as a function of time, either by measuring the mass variation or by analyzing the outlet gas stream.

Ammonia is the most commonly employed probe molecules. Its strong basicity and small size allows it to access even the smaller pores, adsorbing on different types of acid sites. Pyridine is a very strong base which is usually employed but, contrary to ammonia, its bigger dimensions may hinder the access to some sites [15].

In fact, a prior study [32] has concluded that up to 40% of the experimental heat of adsorption of small bases in zeolite micropores measured by calorimetric techniques is originated by confinement effects, related to the physical interactions between the adsorbed base and the zeolite framework. Thus, the true values for the heat of adsorption can only be obtained when this contribution is removed from the experimental data.

Another problem lies on the surface heterogeneity of the sample, which results in more than one type of adsorption sites, with several peaks shown in the thermograms or, more often, with all these peaks being overlapped in a single peak. Additionally, this technique is incapable of distinguishing between Lewis and Brønsted acid sites [15], and the desorption peaks can be significantly different depending on the probe molecule that was used or due to side interactions [9].

Desorption can be either carried out under vacuum or under an inert gas stream (He or N_2), as a way to counteract complications such as the slow diffusion or the readsorption of probe molecules (which creates asymmetric and/or strongly overlapped signal [9]). In fact, the latter proves to be one of the major disadvantages of this technique, as it can strongly affect the results.

Thus, the interpretation of results may prove to be very complex, and complications may ensue even when comparing homologous samples, so reliable results can only be drawn from this technique upon strict control of the experimental conditions.

Several alterations to the experimental procedure have been studied, namely combination of techniques such as IRMS-TPD, which permits the characterization of the acid site structure and the distinction between BAS and LAS by infrared and mass spectroscopy, as well as the distinction between its strength and amount by traditional TPD [9,15].

2.3.1.3 Decomposition of alkylamines

This method is a modification of TPD and uses alkylamines, usually isopropylamine and n-butylamine as their sizes are suitable for many zeolites. This method provide quantitative data on the density of BAS in zeolites, by assuming that each Brønsted acid site forms a complex with one amine

in a 1:1 ratio, which decomposes into olefins and ammonia via the Hoffman elimination (see equations (2.3.1.3.1) and (2.3.1.3.2)) [1,9].

$$RCH_2 - CH_2 - NH_2 + HZ \rightarrow RCH_2 - CH_2 - NH_3{}^+ - Z \qquad (2.3.1.3.1)$$

$$RCH_2 - CH_2 - NH_3{}^+ - Z \rightarrow RCH_2 = CH_2 + NH_3 + HZ \qquad (2.3.1.3.2)$$

As decomposition is selective to BAS, this technique can distinguish between BAS and LAS, but it does not provide information on the acid strength of the sites [9].

2.3.2 Solid-State MAS NMR

Nuclear magnetic resonance (NMR) spectroscopy was discovered in 1945 and its range of applications has steadily grown through time. NMR can be used to study the chemical composition, the structure or location of relevant T-atoms (framework vs. extra-framework species, surface vs. inner sites), balancing metals and protonic acid sites, and it can also be used for adsorption and diffusion studies [9,15].

Magic angle spinning (MAS) completely revolutionized the field of solid-state NMR, as it drastically improved the resolution, closer to that of liquid state NMR. This technique consists in rapidly spinning the sample around an axis forming a specific angle (the magic angle – 54,74°) with the direction of the external magnetic field, to minimize the effects of the immobility of the molecules and anisotropic interactions, as well as to cancel the effect of dipole-dipole interactions [9].

Different nuclei can be studied by MAS-NMR. For instance, ^{29}Si and ^{27}Al determine the concentration acid sites, whereas ^{17}O, ^{1}H, ^{15}N, and ^{31}P provide information on the acid strength of BAS [15].

The ^{29}Si spectrum comprises several peaks originated by silicon nuclei surrounded by a different number of neighboring aluminum atoms (ranging from zero to four) [9,15] and, in smaller proportion and not as often, peaks concerning silanol species (silicon attached to unbridged OH groups). Quantification of these peaks by deconvolution allows the determination of different silicon sites, as well as the aluminum distribution on the structure of the zeolite [15].

On the other hand, ^{27}Al usually contains two distinctive peaks concerning tetrahedral and octahedral structures [19], concerning, respectively, framework aluminum and extra-framework species responsible for the formation of LAS. The aluminum distribution can be measured by the relative intensity of these two signals [9].

Complementing the information obtained on the two aforementioned spectra, it is possible to calculate the Si/Al mole ratio of the samples (not concerning extra-framework species [15]), by employing equation *(2.3.2.5)*, where *I* correlates to the peak intensity and n to the number of neighboring aluminum atoms [9]. This formula works well for low Si/Al ratios, and well crystalized zeolites, but the presence of Si defects may create broad components which overlap the whole signal.

$$\frac{Si}{Al} = \frac{\sum_{n=0}^{n=4} I_{Si(nAl)}}{\sum_{n=0}^{n=4} \frac{nI_{Si(nAl)}}{4}} \qquad (2.3.2.5)$$

^{17}O MAS-NMR allows the distinction between hydroxyl groups from framework non-protonated oxygen atoms. However, it is not very often studied, as the very low natural abundance of this isotope requires the usage of expensive enriched species [15].

^{1}H MAS-NMR spectrum usually shows several peaks originated by hydroxyl groups with different surroundings, with the most interesting being the bridging Si(OH)Al groups, since the proton is catalytically active. Prior to an analysis by this technique, all adsorbed water should be removed, to prevent overlapping of the water protons' bands with those of the hydroxyl groups' protons. The deconvolution of the spectrum gives information on the number of sites and its acidic strength.

Additionally, several studies point to the possibility of establishing an acid strength scale of protons and to determine their relative location by observing the ^{1}H chemical shift, as more unshielded protons (which give higher chemical shifts) will break their bonds more easily, thus, portraying higher Brønsted acid strength [15]. This nucleus is very appealing when compared to others, not only due to its natural abundance, but to the short time required to obtain a detailed spectrum.

^{15}N and ^{31}P MAS-NMR can be additionally used for *in situ* experiments to indirectly detect protonated and non-protonated complexes (respectively BAS and LAS) by means of probe molecule (containing ^{15}N and ^{31}P atoms) interaction [15].

Changes in the NMR signals of the zeolite (like ^{1}H NMR) and of the probe (^{13}C, ^{15}N, ^{3}1P, etc.) occur, with the size, basic strength, flexibility and shape of the probe determining the sites that can be detected. These molecules group in strong Lewis bases that undergo full protonation, and mildly basic molecules that interact by hydrogen bridging and dispersive forces [9]. Examples of common probe molecules are pyridine, carbon monoxide or acetone. Bulkier probe molecule can distinguish between inner acid sites and those on the surface.

However, this technique has its limitations. For instance, it is a very costly technique, due to the probes and to the equipment that is used, and the preparation of the sample/rotor that should be done in a glovebox. Additionally, the low temperatures that are used are different from those employed in catalytic processes, providing misleading conclusions on the performance of the catalyst.

2.3.3 Model reactions

Model reactions offer a reliable alternative to characterize the strength and density of different acid sites, as the employed conditions of analysis is closer to the real catalytic conditions [33]. Additionally, model reactions allow the distinction between BAS and LAS, contrary to information on the total number of sites obtained by most characterization techniques.

However, the acidity of zeolites can only be fully characterized by employing several different reactions, as only the sites reactive to a certain reaction will be characterized. In this sense, a model reaction should be chosen according to the structure of the zeolite and the specific type of site to be studied, while not being sensitive to others and maintaining a nature similar to other model reactions, in order to be comparable between each other. Aside from that, model reactions must have a simple mechanism in order to facilitate the measure of the initial rate (which may prove difficult, as acid catalysts undergo rapid initial deactivation) [15]. Other problems with this technique may be related to confinement effects, which affect the concentration of reactant molecules near the active sites and, consequently, the reaction rate.

Some commonly employed model reactions can be consulted in Table 2.

Table 2: Commonly employed model reactions. T_R – Reaction temperature. Taken from [15]

Reactant	T_R (K)	Reaction
3,3-dimethyl-1-butene	473	Skeletal rearrangement
cyclohexene	473	Skeletal isomerization Hydrogen transfer
2,2,4-trimethylpentane	623	Cracking
2,4-dimethylpentane	623	Isomerization Cracking
2-methylpentane	673	Isomerization Cracking
n-hexane	693	Isomerization Cracking
o-xylene	623	Isomerization Disproportionation
1,2,4-trimethylbenzene	623	Isomerization Disproportionation

2.3.4 General conclusions

In line with what has been previously disclosed, there are roughly three different alternatives to characterize the acidity of solids. For instance, spectroscopic techniques such as FT-IR and MAS-NMR aim to evaluate the strength of the hydroxyl O-H bond and correlate its structure to its properties. These same spectroscopic techniques, as well as calorimetry and TPD, allow the quantification of the interaction of a basic probe molecule with the acidic sites. Finally, catalytic test reactions with variable acid strength requirements can give information on the density of the acid sites, by studying their respective selectivity [15].

Infrared studies mainly concern the characterization of the bands originated by hydroxyl groups, as these portray Brønsted acidity. These studies often employ probe molecules, such as carbon monoxide, ammonia, pyridine, etc. The adsorption of these molecules will provide information on the nature of the acid sites (Brønsted vs. Lewis) and their location (inside small or large pores, framework vs. extra-framework sites).

The main advantage of using perdeuterated benzene over other probe molecules is that the distinction of the acid sites will be obtained on a region of the spectrum devoid of any other species that may contribute to the signal, aside from the hydroxyl groups which have undergone H/D exchange by contact with this probe molecule. In this sense, it wins over other probe molecules which are often not accurate enough to precisely determine the distribution of acid sites, and over many other techniques that cannot provide reliable quantitative results.

(This page was intentionally left in blank)

3 Experimental Part

3.1 Experimental setup

Infrared spectra with a range between 4000 and 400 cm^{-1} were recorded in transmission mode using a *ThermoFischer Scientific Nicolet iS50* FT-IR spectrometer, equipped with a KBr beamsplitter and a DTGS (Deuterated Tryglicine Sulfate) thermal detector. Each spectrum was recorded with a resolution of 4 cm^{-1}, accumulating 40 scans per spectrum.

Aside from the previously mentioned instrument, common laboratory material was employed to carry out the *in-situ* adsorption of the gas phase probe molecule. Additionally, the samples pressed in the form of wafers were weighted in a *Mettler AE 163* analytical balance, and the primary and secondary vacuum were provided by two *Edwards* vacuum pumps, to obtain pressures in the order of 10^{-6} mbar.

A schematization of the employed experimental setup can be consulted in Figure 4. A detailed illustration of the used sample holder is represented in Figure 5.

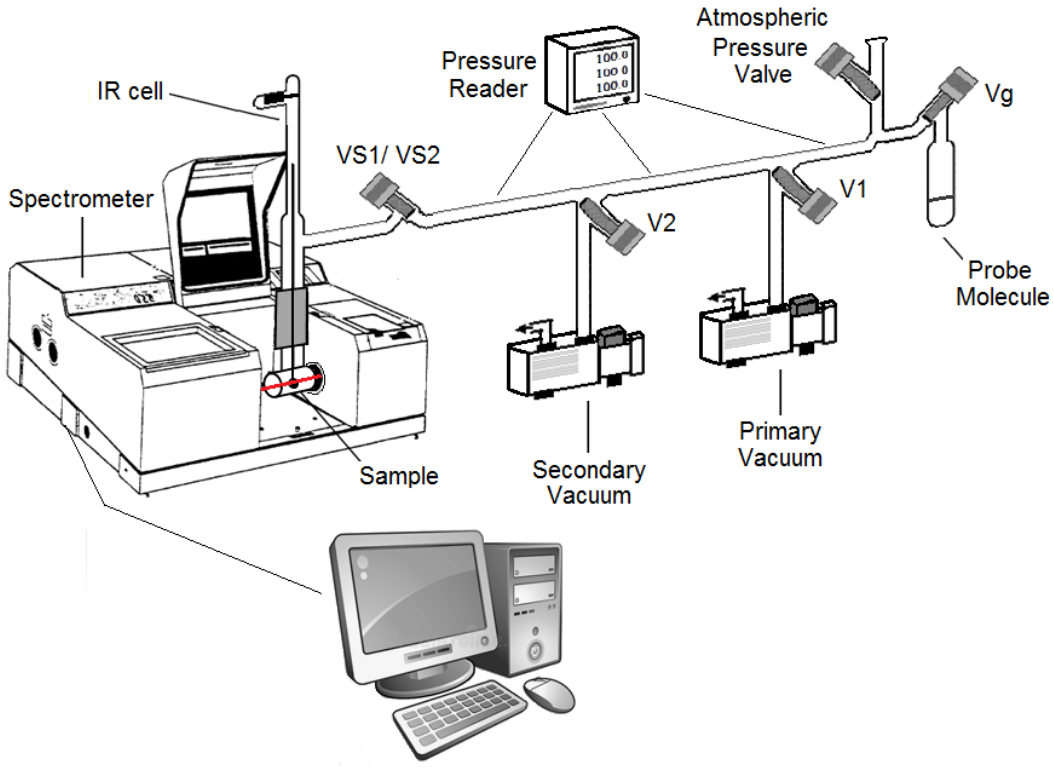

Figure 4: Simplified schematization of the employed experimental setup. Adapted from [7]

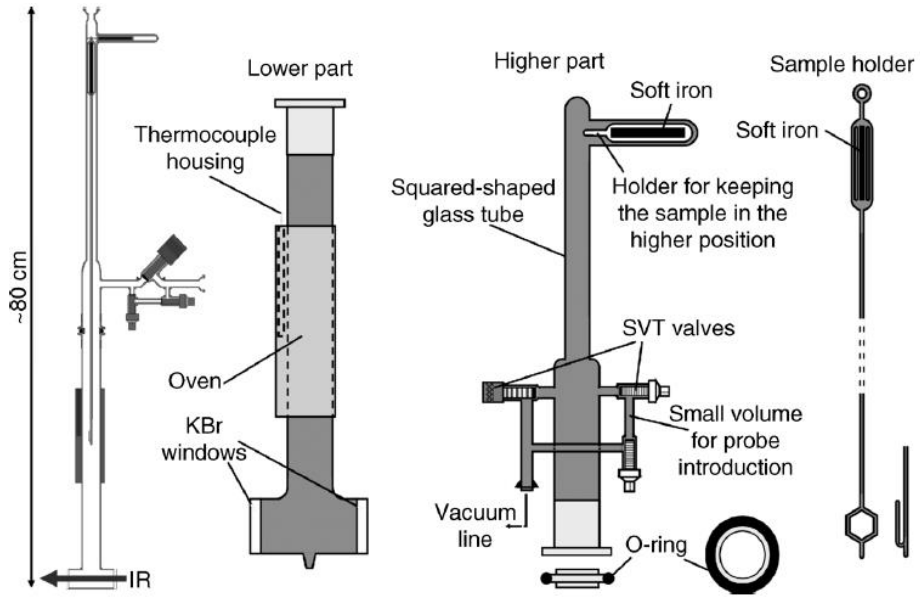

Figure 5 : Scheme of a sample holder used in spectroscopy studies. Taken from [14]

As seen in Figure 4, the setup consists of a FT-IR spectrometer, equipped with a sample cell coupled with a programmable oven. Several valves are connected to the sample holder in order to regulate the vacuum and the vapor pressure of probe molecule circulating in the setup. The probe molecule is contained in a glass ampoule, previously filled with liquid C_6D_6 (*Sigma Aldrich*, 99,6 atom % D). The amount of probe molecule introduced can be directly regulated by the glass ampoule's valve, Vg. Valves V1 and V2 ensure the communication with the primary and the secondary vacuum pumps, respectively.

The sample cell shows two valves, named VS1 and VS2, responsible for connecting the interior of the sample cell with the rest of the setup. The contact with probe molecule was processed in the following manner: the primary and the secondary vacuum were turned off by closing valves V1 and V2. Valve Vg was opened until the amount of C_6D_6 introduced accounted for a vapor pressure of approximately 20 mbar equilibrium. Valves VS1 and VS2 were opened in order to introduce C_6D_6 in the sample cell, closed when the equilibrium pressure reached ~5 mbar. Valve V1 was opened to evacuate the probe molecule circulating in the remaining parts of the setup. When the time for contact ended, valves VS1 and VS2 were opened, followed by closing valve V1 and opening valve V2 to carry out evacuation under secondary dynamic vacuum.

The quartz sample holder could be moved up or down with the aid of a magnet positioned at the top. It would be moved up when performing activation or contact with probe molecule at 150°C, so that the wafer could be heated up inside the oven (see Figure 5). On the contrary, it would be moved down and aligned with the IR beam, when a spectrum was to be recorded or when contact with C_6D_6 at room temperature was performed.

3.2 Experimental procedure

3.2.1 Preparation of the wafer

In order to carry out the experiments, approximately 20 mg of pure sample were pressed into a self-supporting wafer with a surface area of ~ 2 cm^2. The pressing pressure was kept at 2 ton during 30 seconds in a *Specac Atlas Autotouch 8T* presser. This is a crucial step as the wafer should be thin enough to remain transparent in the mid-IR region and to prevent noisy and non-quantitative results, and should be gently pressed, as the usage of higher pressures, albeit facilitating the preparation of the wafer, can damage the structure of the solid or hinder the gas diffusion and adsorption of probe molecules during analysis. Additionally, the wafer should have an homogenous thickness, in order to acquire reliable data, as it can alter the optical path of the infrared beam and, thus, the collected signal.

3.2.2 Activation of the wafer

The self-supporting wafer was placed inside a transmission cell with KBr windows and a controlled atmosphere, where it was subjected to an activation step aiming at the removal of unwanted surface species such as physisorbed water. This was done by using a programmable oven.

The first step (see Figure 6) consisted of heating up the sample from room temperature up to 100°C and keeping it at this temperature for at least one hour. A ramp step would follow, to increase the temperature up to 450°C. This temperature was kept for a minimum duration of 10 hours. The last step was to decrease the temperature back to 100°C, which was kept until the beginning of the experiment to prevent readsorption of water. Note that the activation procedure has been performed in dynamic conditions under secondary vacuum with pressures around 10^{-6} mbar inside the cell.

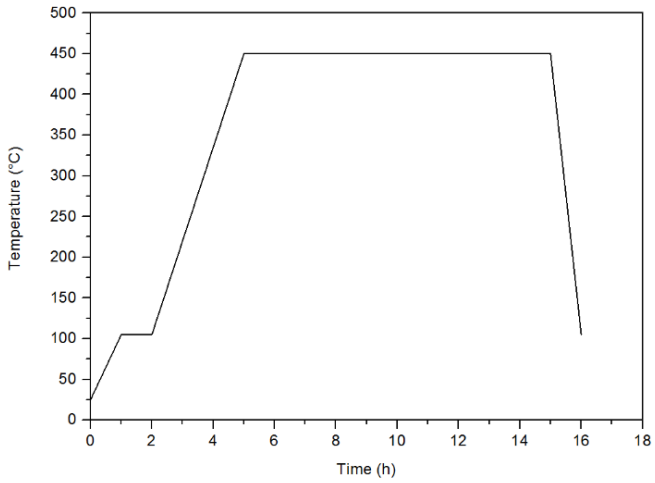

Figure 6: Typical temperature program employed during the activation process. Note that what is represented in the figure is the minimum duration of each step

3.2.3 Contact with probe molecule

A background spectrum was recorded after thermal activation. Prior to contact with C_6D_6, an initial spectrum of the activated sample was also obtained. The sample was then put in contact with the probe molecule at room temperature, at first for 30 seconds. Contact times of 5 minutes and 10 minutes followed (with contacts of 20 minutes and 30 minutes for some of the samples). An evacuation step of approximately 15 minutes under dynamic secondary vacuum (pressure below 10^{-6} mbar) followed every contact in order to remove the excess C_6D_6 inside the setup, with a spectrum being recorded at the end of each of these steps. Note that the evacuation time for CBV500 and its calcined form required approximately 1 hour.

Some samples were heated up to 150°C. In this case, the contact with the probe molecule was done by successive periods with a fixed duration of 15 minutes, followed by 15 minutes evacuation. Analogous with the procedure at room temperature, a spectrum was recorded at the end of each evacuation step.

A global schematization of the experimental procedure is given by Figure 7.

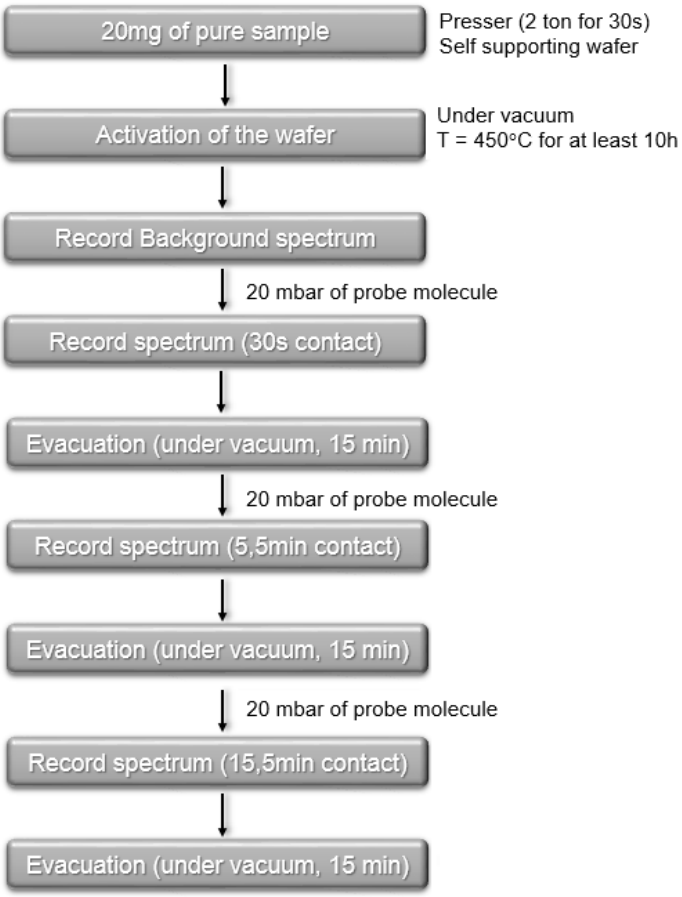

Figure 7 : Schematization of the employed experimental procedure

4 Problems and difficulties

Prior to discussion of the collected results, it is necessary to briefly explain how the data treatment was carried out. Spectra obtained by infrared spectroscopy are most frequently subjected to deconvolution, in order to distinguish between the different acid sites that are contributing to the resulting spectrum (overlapping contributions), and as a mean to obtain their relative quantification by integrating the area below each deconvoluted curve. Thus, this type of data treatment allows the attribution of distinctive bands to their correlated functional groups, and their quantification, which is commonly applied in spectroscopic studies.

Deconvolution was the first tested methodology to develop a data treatment that could be reproducible and applicable to all the studied samples. However, the changing position of the bands due to the different characteristics in each type of tested zeolite gave non-comparable quantitative results between distinct samples. Additionally, deconvolution proved to be a very onerous task as the Si/ Al ratio increased.

Direct area integration was posteriorly applied, posing as a solution to the limitations found when trying to deconvolute the spectra. For this technique, a baseline is chosen between the wavenumbers of interest. By using it as reference, the area concerning a specific range of wavenumbers comprised in the baseline can be directly taken, hence its terminology. Nevertheless, the tilting of the spectra was still not corrected.

This leads to the final treatment employed in the present report, and which has been used to treat all the data that will be disclosed in the following pages.

Fourier Self-Deconvolution is a method that has been developed since the 1980s as a computer processing of spectral data, specifically of proteins [13]. It uses Fourier transforms and is comparable to first-order derivatives, allowing to study intrinsically overlapped band contours [34]. This method enhances the visualization of individual IR bands and suppresses baselines difficulties, but it does not improve the resolution. Furthermore, it cannot resolve an IR band into a single component unless this individual component was present in the original spectrum.

Two factors play a fundamental role on the quality of the information taken by applying this method, being the line bandwidth (BW) and the enhancement factor (EF), which can be defined as the width of the spectral line at half-height and the ratio of line bandwidth before and after deconvolution, respectively. Another factor that should not be overlooked is the signal to noise ratio (STN) of the original spectrum, as it should be appropriately high to enable the resolution of the spectrum into individual components [13], without enhancing the noise.

The first step in order to correctly employ this method is to find the optimal values for each of these parameters, that will enhance the individual signals overlapped in each type of samples. Optimal values for these parameters can be found in the literature, with a BW of 22 cm^{-1} and EF of 3.0 for mordenite zeolites [13].

Using these as a starting point to obtain the optimal parameters, EF values were first changed between 3 and 0, while BW was fixed at 22 cm^{-1}. As observed on the left side of Figure 8, the EF value mentioned in the literature will create very narrow bands, while lower values than 2 will lead to broad bands, thus deleting some of the information. Hence, the best value to use appears to be 1,5.

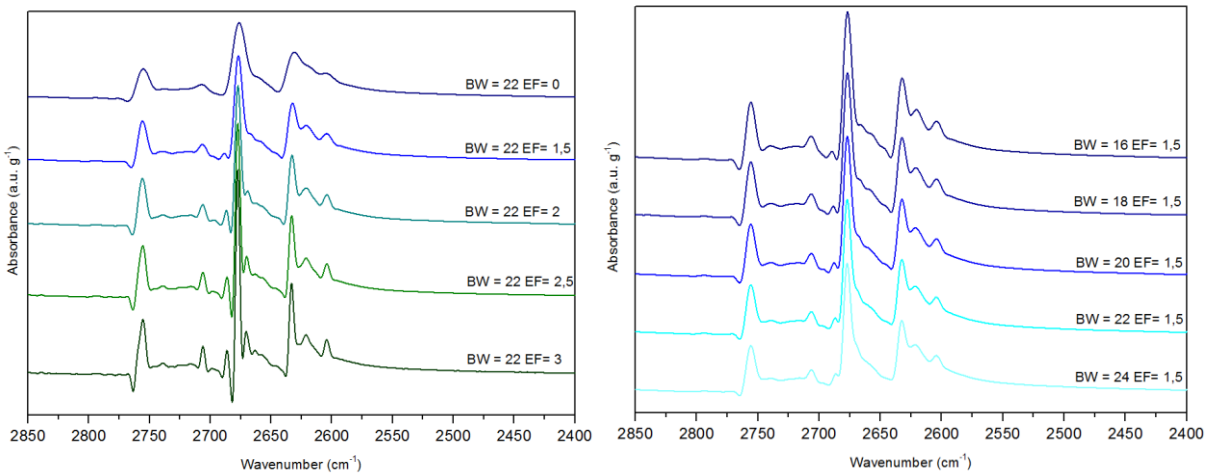

Figure 8 : Effect of EF keeping BW at 22 cm^{-1} (left) and effect of BW keeping EF at 1,5 (right) for a zeolite FSD treated spectra

Keeping this value fixed for EF and changing BW between 16 cm^{-1} and 24 cm^{-1}, it is concluded that the positions and number of the single bands are strongly influenced by this parameter (see band shift on the right side of Figure 8), in conformity with what has been previously observed [13]. When decreasing BW, very short bands will be enhanced, while the opposite occurs when this parameter is increased. A compromise was made and a value of 20 cm^{-1} was chosen for BW. The final parameters used for the zeolitic samples were an EF of 1,5 and a BW of 20 cm^{-1}.

Figure 9 shows the spectra of CBV720 after different contact times with C_6D_6 before and after applying FSD. When observing the latter, it is clear that the preexistent bands are much more defined, and the contributions of the different acid sites are more pronounced.

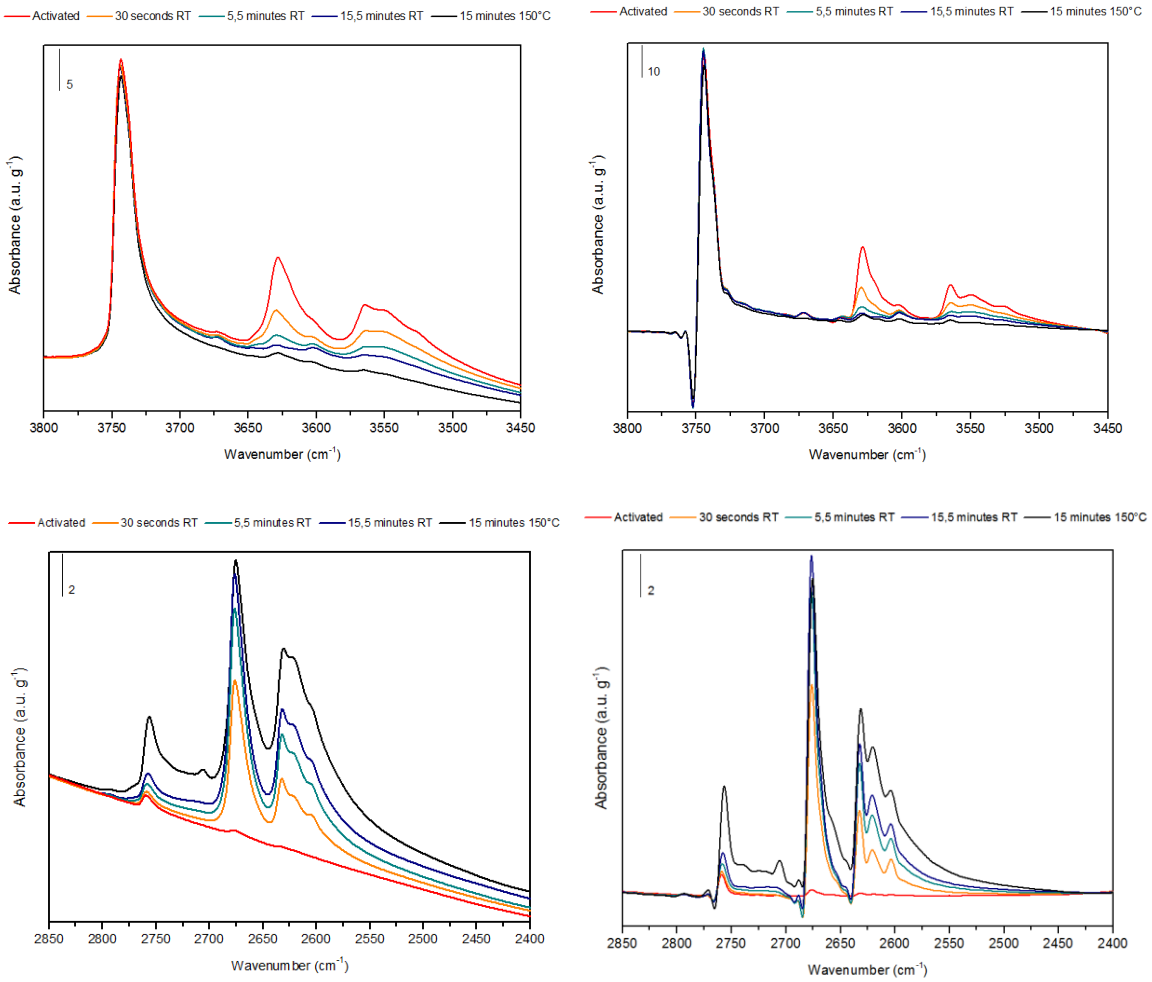

Figure 9 : Spectra comparison in the hydroxyl (top) and in the deuteroxyl region (bottom) of CBV720 before (left) and after (right) Fourier Self Deconvolution

This method also proves to be useful when dealing with samples with lower Si/Al ratio (CBV500, Figure 10). However, the effect of FSD is not as prominent as the expression of the overlapped bands is not as intense.

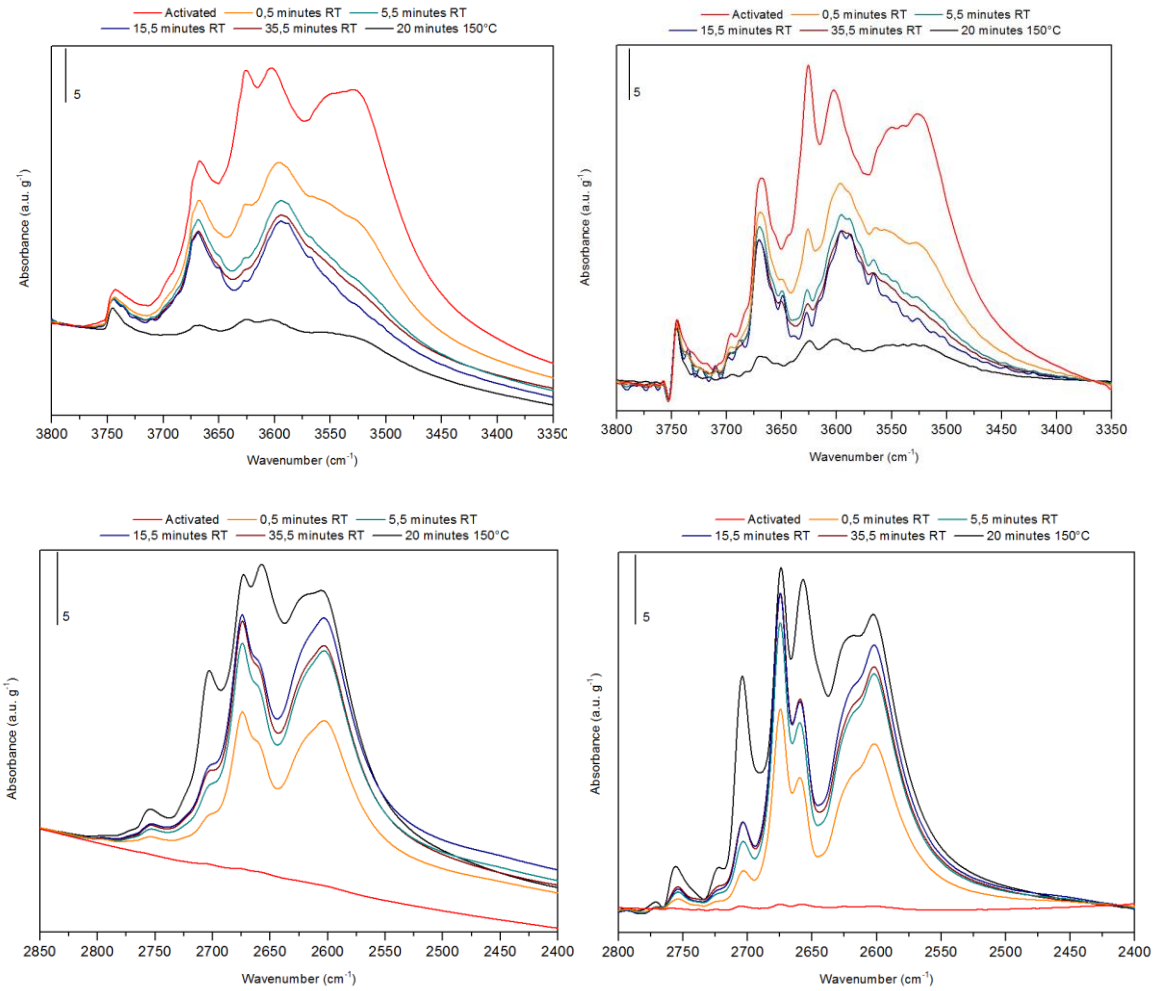

Figure 10 : Spectra comparison in the hydroxyl (top) and in the deuteroxyl region (bottom) of CBV500 before (left) and after (right) Fourier Self Deconvolution

One of the biggest advantages when employing this treatment is the correction of the baseline. As all spectra are treated in the same manner, the quantification of the acid sites can be easily performed by direct integration, not only for spectra concerning different exchange times on the same sample, but when comparing different types of samples as well.

As above-mentioned, this method was developed to study the structure of proteins, so few studies have been published when concerning other compounds, thus making the application of FSD on faujasite zeolites a novelty. In conclusion, and in line with what was previously mentioned, FSD-IR provides unprecedented research advantages unmatched by other techniques on the treatment of infrared spectra for these acid solids.

5 Results on zeolites

5.1 Experimental Section

In order to validate the technique employed in the present report, an extensive series of zeolites was characterized. The reasoning behind choosing each of the samples and which effects could be studied on them will be addressed in the following pages.

5.1.1 Description of the samples

Faujasite zeolites were studied in the present work. Commercial zeolites provided by *Zeolyst* and without any posterior modification were characterized. These zeolites ranged from CBV500, a purely microporous Y zeolite in its ammonia form, to CBV760, a mesoporous zeolite in its protonated form. These zeolites have been subjected to post-synthesis treatments, namely calcination, steaming and shaping procedures. The resulting supports have been characterized and compared to its parent zeolites. Table 3 summarizes all the samples provided by *Zeolyst* which were characterized.

Table 3 : Overview of commercial faujasite zeolites from *Zeolyst*. Adapted from [21]

CBV code	Sio_2/Al_2O_3 Mole Ratio	Si/Al (mol mol^{-1})	Cation	NaO_2 Weight %	Unit cell size (Å)	Surface Area (m^2 g^{-1})	Supposed Treatments
500	5,2	2.6	NH_4^+	0,2	24,53	750	Ion exchanged Mildly steamed
712	12	6	NH_4^+	0,05	24,35	730	Ion exchanged Moderately steamed Acid treated (leaching)
720	30	15	H^+	0,03	24,28	780	Ion exchanged Severely steamed
760	60	30	H^+	0,03	24,24	720	Ion exchanged Severely steamed Acid treated

5.1.1.1 Detailed explanation of the different series and studied effects

Different series of zeolites have been studied in order to determine how and to which extent different parameters affect the surface acidity of zeolites and its catalytic performance.

One of the most important parameters that influences the acidity of zeolites is its silicon to aluminum ratio (Si/Al). As stated previously, zeolites are porous solids containing Lewis and Brønsted

acid sites, with the former sites relating to coordinatively unsaturated sites working as electron acceptors, and the latter being related to surface hydroxyl groups (attached to the zeolitic framework).

These hydroxyl groups are the direct result of the AlO_4 tetrahedra bearing a negative charge, and the need of compensating cations, as protons for instance, to ensure the electroneutrality of the zeolite framework. These cations are easily exchanged and substantially influence the acid sites present in zeolites.

As the content of aluminum increases in a catalyst, a larger quantity of compensating cations will be present and, logically, more acid sites will be created. Thus, as the silicon to aluminum (Si/Al) ratio decreases, the more will be the acidic behavior of the zeolite. In line with these arguments, the first series to be characterized comprises zeolites with a Si/Al ratio ranging from 5 to 60 and with different compensating cations in their framework.

Post synthesis modification was also studied, mainly related to dehydroxylation and dealumination by employing high temperature calcination and to structural modifications by steaming procedures. As such, the effect of calcination will be studied by comparing the calcined forms of CBV500 and CBV712 to their respective parent samples. Not only will it be possible to draw conclusions on how calcination alters the acidity on these two samples, it will also shed light on how porosity is affected by this treatment, both on CBV500 and CBV712, respectively microporous and mesoporous zeolites.

In addition, CBV720 has been dealuminated by two different routes: by conventional steaming and by acid treatment in liquid phase. The differences in extent and type of dealumination on these two samples will be compared, as well as with the respective parent zeolite.

When a zeolite undergoes dealumination, a great part of its framework Al is removed. These species can be removed from the material by acid treatments or remain at its surface as extra-framework species. Severe dealumination triggers two conflicting effects in the catalyst: as the aluminum is removed, the overall acidity of the sample decreases substantially but not in a uniform way, as the extra-framework Al species favor the formation of acid sites of enhanced acidity (known as perturbed acid sites). A decrease of crystallinity can also occur.

Afterwards, the shaping effect on CBV720 will also be studied. For this, both the commercial CBV720 and the modified sample obtained by dealumination employing acid treatment will be mixed with an alumina binder. The results will then be compared with the aforementioned non-shaped samples. Advantages of shaping a zeolite can be found on the literature but, briefly contextualizing, zeolites can be mixed with an alumina binder or with amorphous silica alumina. By using alumina, it is intended to shape the zeolite in order to dilute it in the catalyst and to manipulate it in such a way that allows the filling of the reactor, while decreasing the plug tendencies of using zeolite powder alone. Shaping with amorphous silica alumina allows the optimization of the acidity. Thus, shaping a catalyst can refine its properties in terms of selectivity and acidic strength, resulting in “tailor made” zeolites portraying increased performances for a specific application.

5.1.2 Complementary information on the tested zeolites

Table 4 summarizes complementary information drawn from commercial characterization techniques. Specifically, N_2 physisorption allowed the determination of the microporous surface (S_μ) per mass unit, by subtraction of the external surface (S_{ext}) from the obtained BET surface value (S_{BET}). Despite not being applicable to microporous samples, the results obtained for CBV500 have been included for comparison purposes. Values concerning the total acidity measured by pyridine adsorption will be useful in the upcoming chapter where the concentration of the acid sites obtained when using this probe molecule and C_6D_6 will be compared. Both the values concerning Brønsted and Lewis acid sites quantified by pyridine adsorption have been added in the present report.

Table 4 : Complementary information (pyridine adsorption and N_2 physisorption)

Sample	Pyridine Adsorption			N_2 physisorption		
	Brønsted Area (a.u g^{-1})	**Lewis Area (a.u g^{-1})**	**Total Area (a.u g^{-1})**	**S_{BET} (m^2 g^{-1})**	**S_{ext} (m^2 g^{-1})**	**S_μ (m^2 g^{-1})**
CBV500	584	206	790	827	85	742
Calcined CBV500	346	288	634	824	65	759
CBV712	250	197	447	845	147	698
Calcined CBV712	216	187	403	782	105	677
CBV720	188	120	308	923	253	670
CBV720 2nd batch	163	110	273	885	256	629
Steamed CBV720	46	84	130	850	185	665
Modified CBV720	50	21	71	928	276	652
CBV760	136	38	174	867	239	628

5.2 Results and Discussion

5.2.1 Band attribution

The band attribution for the hydroxyl region can be consulted in Figure 11 and in Table 5.

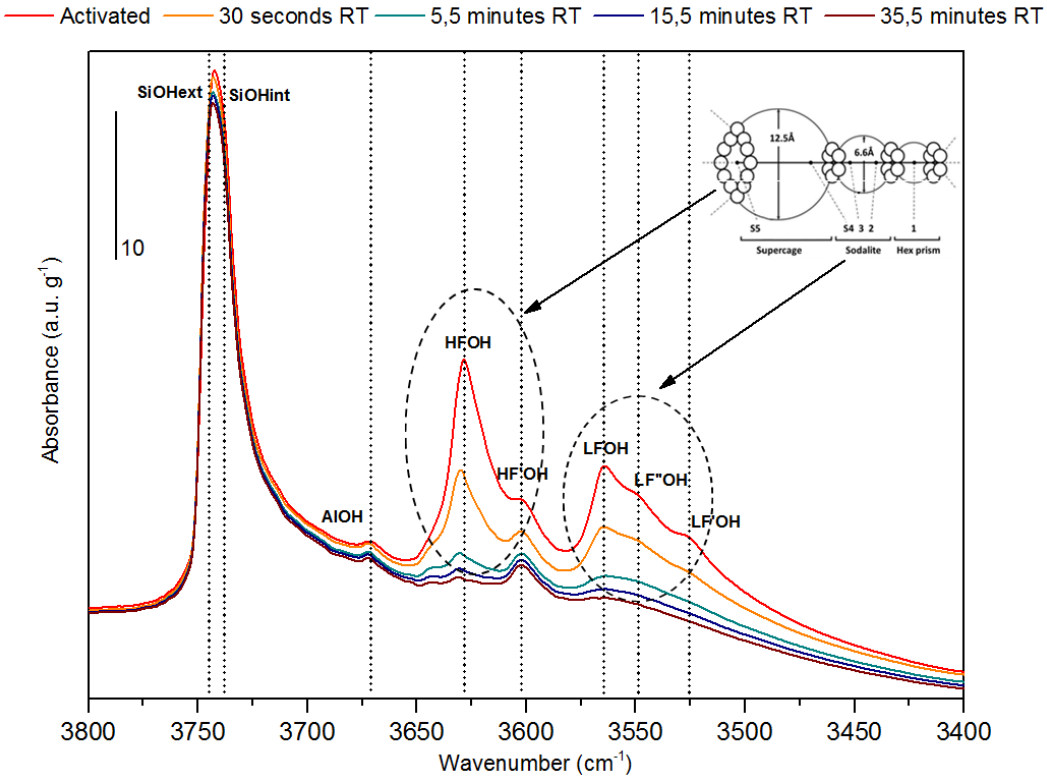

Figure 11 : Band attribution for the hydroxyl region of CBV720. Different spectra after contact with C_6D_6 are represented

Table 5 : Band attribution of different acid sites in zeolites for the hydroxyl region

Hydroxyl type	Definition	ν(OH) (cm^{-1})
External SiOH	SiOHext	3745
Internal SiOH (Perturbation Si(OH)…Al)	SiOHint	3736
Partially extra-framework AlOH	AlOH	3670
Supercage framework Si(OH)Al	HFOH	3629
Sodalite cage framework Si(OH)Al	LFOH	3564
Perturbed Si(OH)Al by extra-framework Al	HF'OH	3602
	LF"OH	3550
	LF'OH	3525

As the H/D exchange unfolds, the signal previously seen in the hydroxyl region is shifted to lower wavenumbers (the deuteroxyl region) due to the heavier mass of deuterium compared to the

proton. The ratio between the wavenumbers of the bands in the hydroxyl and the deuteroxyl region is of ~1,35.

Once more using CBV720 as an example, the band attribution in the deuteroxyl region can be consulted in Figure 12 and Table 6.

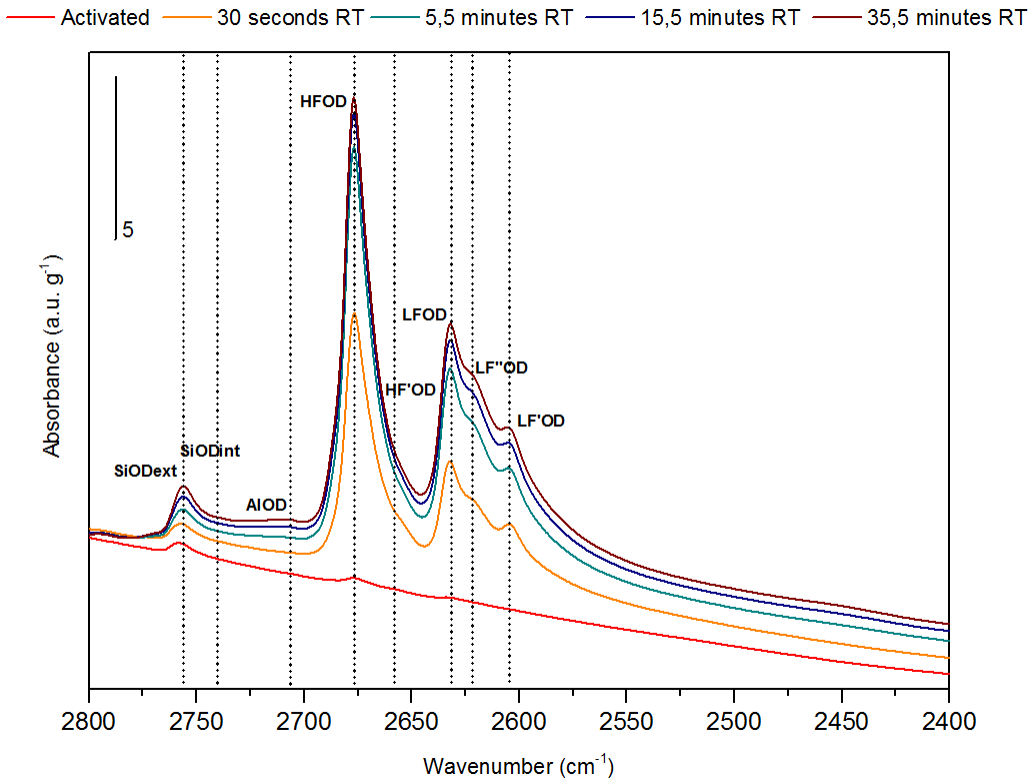

Figure 12 : Band attribution for the deuteroxyl region of CBV720. Different spectra after contact with C_6D_6 are represented

Table 6 : Band attribution of different acid sites in zeolites for the deuteroxyl region

Deuteroxyl type	Definition	v(OD) (cm^{-1})
External SiOD	SiODext	2762
Internal SiOD (Perturbation Si(OD)…Al)	SiODint	2755
Partially extra-framework AlOD	AlOD	2706
Supercage framework Si(OD)Al	HFOD	2676
Sodalite cage framework Si(OD)Al	LFOD	2628
Perturbed Si(OD)Al by extra-framework Al	HF'OD	2656
	LF"OD	2618
	LF'OD	2599

5.2.2 Si/ Al ratio

As previously stated, the first parameter subjected to study was the silicon to aluminum ratio of the zeolites. The FSD treated spectra of the activated samples and after contact with C_6D_6 for the hydroxyl and deuteroxyl region are provided in Figure 13.

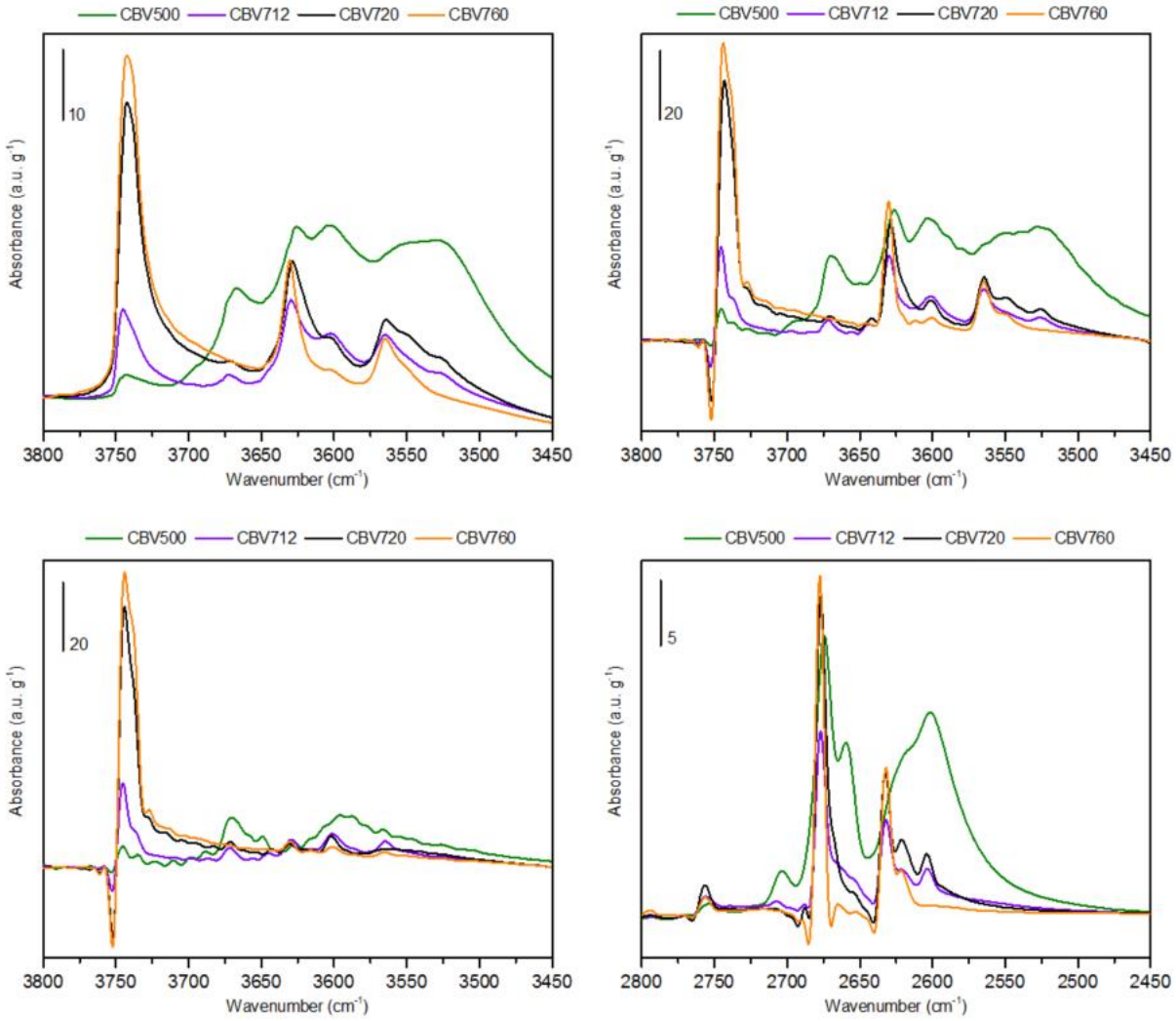

Figure 13 : Si/Al effect on different faujasite zeolites. Activated spectra before (top left) and after FSD treatment (top right) and after 15 minutes contact with C_6D_6 for the hydroxyl region (bottom left) and for the deuteroxyl region (bottom right)

Starting out by comparing the activated spectra, a striking difference can be reported between the spectrum of CBV500 and the remaining zeolites. A possible explanation to this observation might be the presence of NaOH species and a higher concentration of aluminols due to extraframework species at 3670 cm^{-1}. A much weaker silanol signal can be reported on CBV500, in line with its lowest Si/Al ratio and low mesoporosity.

When observing the FSD spectra obtained for the deuteroxyl region, it is clear that this sample displays the highest concentration of stronger acid sites, i.e. HF'OH and LF'OH sites, out of all the zeolitic samples. However, it seems that a larger distribution of strong acid sites is present, opposed to very demarked bands related to LF'' and LF' (at 2618 cm^{-1} and 2600 cm^{-1} respectively) observed on both CBV712 and CBV720. On a side note, this sample appears to contain the greatest number of perturbed sites present in the supercages, judging by the very noticeable shoulder at 2660 cm^{-1} (corresponding to the band at 3600 cm^{-1} found in the activated spectrum).

As a last observation concerning CBV500, a part of the acid sites found on the activated spectra do not undergo H/D exchange with the probe molecule after 15 minutes contact at room temperature. The wavenumbers at which the bands appear correspond to those found on the other less acidic samples (3670-3660 cm^{-1}). Furthermore, it can be concluded that a part of this contribution these bands relate to extra-framework aluminols (~3660 cm^{-1}), as well as to a broad range of acid sites falling in the wavenumbers of Brønsted acid sites (namely HFOH and LFOH), with a broad band with a significant tail at ~3600 cm^{-1}.

It would be expected to see the almost total exchange of perturbed acid sites (HF'OH, LF''OH and LF'OH) after 15 minutes contact with C_6D_6, as these portray higher acidity. However, despite being somewhat difficult to discern in Figure 13, a considerable portion of these sites has not undergone exchange, and the ratio of total exchanged sites is lower than the ones for HFOH and LFOH. These results may be a consequence of a better accessibility for these latter groups, thus exchanging faster, despite the lower acid strength. In fact, this hypothesis is reasonable in the case of LF''OH and LF'OH, the perturbed sites in the sodalite cage, as the H/D exchange occurs by secondary means such as proton/deuteron migration between LF and HF groups, and possibly due to an established equilibrium between (HF)OH/(LF)OH distribution and hopping of a proton from one oxygen site to another in the same aluminum-occupied oxygen tetrahedron [1]. Still, as the exchange occurs by direct contact in the supercage, why HF undergoes exchange at a higher rate than HF' remains unanswered.

When shifting the attention to CBV760, it can be easily concluded that this is the less acidic zeolite, in line with its highest Si/Al ratio. The reasoning comes from the overall less intense bands in the activated spectrum related to the enhanced acid sites, namely the almost imperceptible shoulder for HF' and LF'' and the lacking LF' band. The same observations can be backed up by the spectra of the deuteroxyl region after 15 minutes contact with C_6D_6. Looking closely into the remaining acidic bands, it seems that a part of the perturbed acid sites is gained back as HF and LF sites, as can be discerned when comparing the thinner and more intense bands related to HF and LF sites with the analogous bands collected for CBV712 and CBV720. The highest silanol band can also be reported for this sample, as a result of its higher mesoporosity and high Si/Al ratio.

It appears that the acid sites in this sample, albeit in smaller quantities, undergo almost full H/D exchange after 15 minutes contact with the probe molecule, a result of the open mesoporous structure found in this sample. In fact, when looking at the spectra of CBV712 and CBV720, remnants of the HF and LF bands can still be discerned after 15 minutes contact with probe molecule. This leads

to the conclusions that the acid sites found on CBV760 are more accessible and/ or stronger than in others, which might be a direct consequence of the treatments it was subjected to (see Table 3).

Some differences can be discerned when looking closely at CBV712 and CBV720. In line with what was addressed for CBV760, it seems that the decrease of acidity when going from CBV712 to CBV720 creates a sharper and more intense band for HF acid sites, at the expense of the perturbed HF' sites of higher acidity. This can also be pointed out for the very pronounced increase of intensity reported for the silanol contribution found in CBV720. In addition, the same trends can be found for the spectra after 15 minutes, with CBV720 appearing to exchange more acid sites than CBV712.

In fact, a somewhat significant intensity disparity can be found for the LF'' and LF' bands between these two samples. CBV720 appears to contain more perturbed low frequency acid sites than CBV712 (in theory the most acidic sample of the two). These results may be explained by the treatment performed on CBV720. This sample has been subjected to acid leaching which, despite increasing the Si/Al ratio, keeps the framework ratio, thus creating a more mesoporous sample which possibly allows quicker H/D exchange.

Quantitative results will be useful to validate and to explain some of the observations taken from the spectra (to see how these were calculated, refer to Appendix C). For instance, the trend is not the same when looking at the total acidic OH (HF, HF', LF,LF' and LF'') available to be exchanged on the activated spectra and the respective total OD that has been created after 15 minutes exchange for each of the samples (see top left and right of Figure 14). The total acidic OH available for exchange decreases with the increasing Si/Al ratio, which is in line with the decrease of aluminum.

Looking at the total OD that has been created after exchange, there is a decrease when coming from CBV500 to CBV712, concomitant with the loss of acidity when the Si/Al ratio increases. Nevertheless, as the Si/Al increases, the OD concentration also increases. Thus, the dealumination process that unfolds when the Si/ Al increases may not affect all acid sites in the same manner, with the strong acid sites being kept intact. So, despite the samples having less acidity, the acid sites that remain as the ratio increases are those of stronger acidity, resulting in a higher proportion of OD being created.

One way to validate this hypothesis is by calculating the ratio between the total OD formed after 15 minutes at room temperature and the total acidic OH available in the activated spectra, as a function of the Si/Al ratio. The results can be seen on the bottom left side of Figure 14. Taking into account the found trend, it is reasonable to say that there is an increase in the proportion of stronger acid sites prone to exchange at room temperature.

The quantitative results obtained when using pyridine as a probe molecule are included in the bottom right side of Figure 14. The trend found in this case is concomitant with the one obtained for the total acidic OH, but not with the total OD formed after 15 minutes contact at room temperature.

These conclusions may be a result of the different experimental procedure when using pyridine or C_6D_6 as a probe molecule. For the former, the first contact is performed at 150ºC, thus

providing information on all the acid sites that can be exchanged at that temperature. Since the exchange is started at room temperature when using C_6D_6, the first information to be acquired is related to the concentration of strong acid sites that can be exchanged and, as the temperature increases, acid sites of lower acidity will start to exchange.

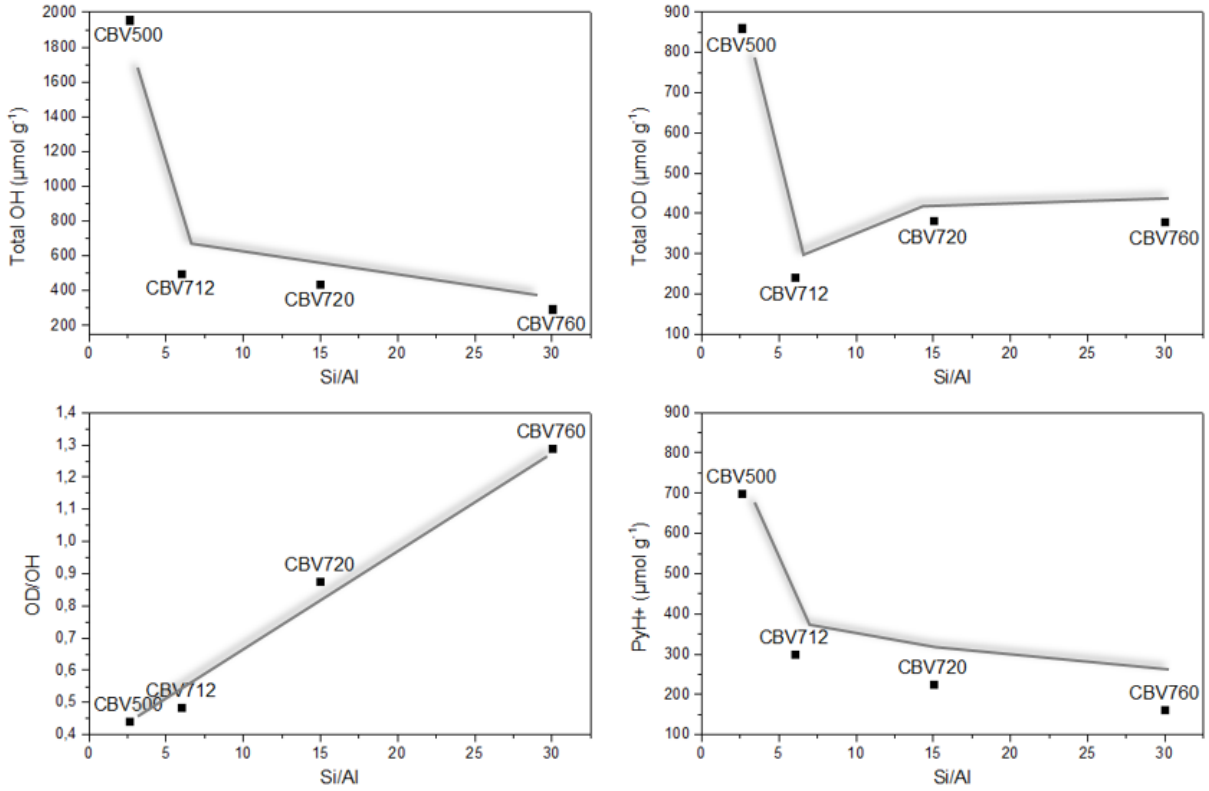

Figure 14 : Quantitative results on faujasite type zeolites according to its Si/Al. Concentration of total acidic OH on the activated spectra on the top left and total concentration of OD exchanged after 15 minutes contact at room temperature on top right. Ratio between OD created and total OH available on the bottom left, pyridine results on bottom right

5.2.3 Calcination effect

The effect of calcination has been studied for two different types of NH_4 form Y and USY zeolites, CBV500 and CBV712. The results can be consulted in Figure 15.

Starting out by the activated spectra and comparing it to the homonymous activated spectra of the calcined samples, a loss of acidity can be reported on both samples. This is especially true for CBV500, as a great part of the intensity of the bands concerning HF and LF is lost. It seems as well, that there is a different site distribution compared to before calcination, observed in the higher intensity of the HF' sites on the calcined sample, in opposition to the reported for CBV500. A much lower LF' shoulder can also be distinguished for the calcined CBV500.

An increase of the silanol groups occurs when calcination is performed. An explanation for these observations lies on the fact that CBV500 is not an USY zeolite, thus not stable upon calcination. During calcination, a part of the micropores is lost, hence the destruction of a part of the acid sites and the creation of silanol groups. The band at 3670 cm^{-1} is also greatly reduced after calcination of CBV500, confirming the attribution of this band to Brønsted acid sites. Calcination alters the microporosity of the sample, which explains why the most evident changes are reported for the acid sites in the LF and LF' range (also backed up by the quantitative results on Figure 16), which are those found in the sodalite cages.

The aforementioned tendencies are not visible for CBV712, as calcination does not result in any substantial differences in these bands. In fact, the overall loss of acidity on CBV712 doesn't appear to be as extreme as what was envisioned for CBV500, as this is an USY zeolite.

When looking at the spectra taken after 15 minutes exchange, it seems that a higher amount of LF sites do not undergo H/D exchange for the calcined sample. Thus, the only possible outcome of having lower and less accessible acid sites to exchange are much less intense bands observed in the deuteroxyl region of this sample.

The calcined form of CBV712 also displays a lower intensity of the extra-framework aluminum band (3670 cm^{-1}). Nevertheless, the thermal calcination of CBV712 seems to have affected all acid sites in the same proportion when looking at the activated spectra. However, when looking at the deuteroxyl region of the spectra for the CBV712 samples, there isn't much of a loss on the HF and LF groups, which leads to believe that the sites lost upon calcination are not exchangeable at room temperature (i.e. weak acid sites), thus resulting in few differences between the calcined and the non-calcined spectra. The exact opposite happens for the perturbed HF' and LF' sites. In fact, the behavior found for most acid sites is similar, but a very pronounced HF' shoulder comprising, seemingly, two different contributions, can be found on the calcined sample, different from the sloped contribution found on CBV712. The shape of this specific band is familiar, as it is similar to the one found in CBV760.

The observations made in this section are concomitant with what is aimed to obtain by calcination. As previously mentioned in section 2.1.1, this treatment is responsible for the thermal decomposition of the active agents' precursors, with modification of the surface and textural properties. However, the calcination temperature should not be too high, as major structural alterations can be introduced in the zeolite.

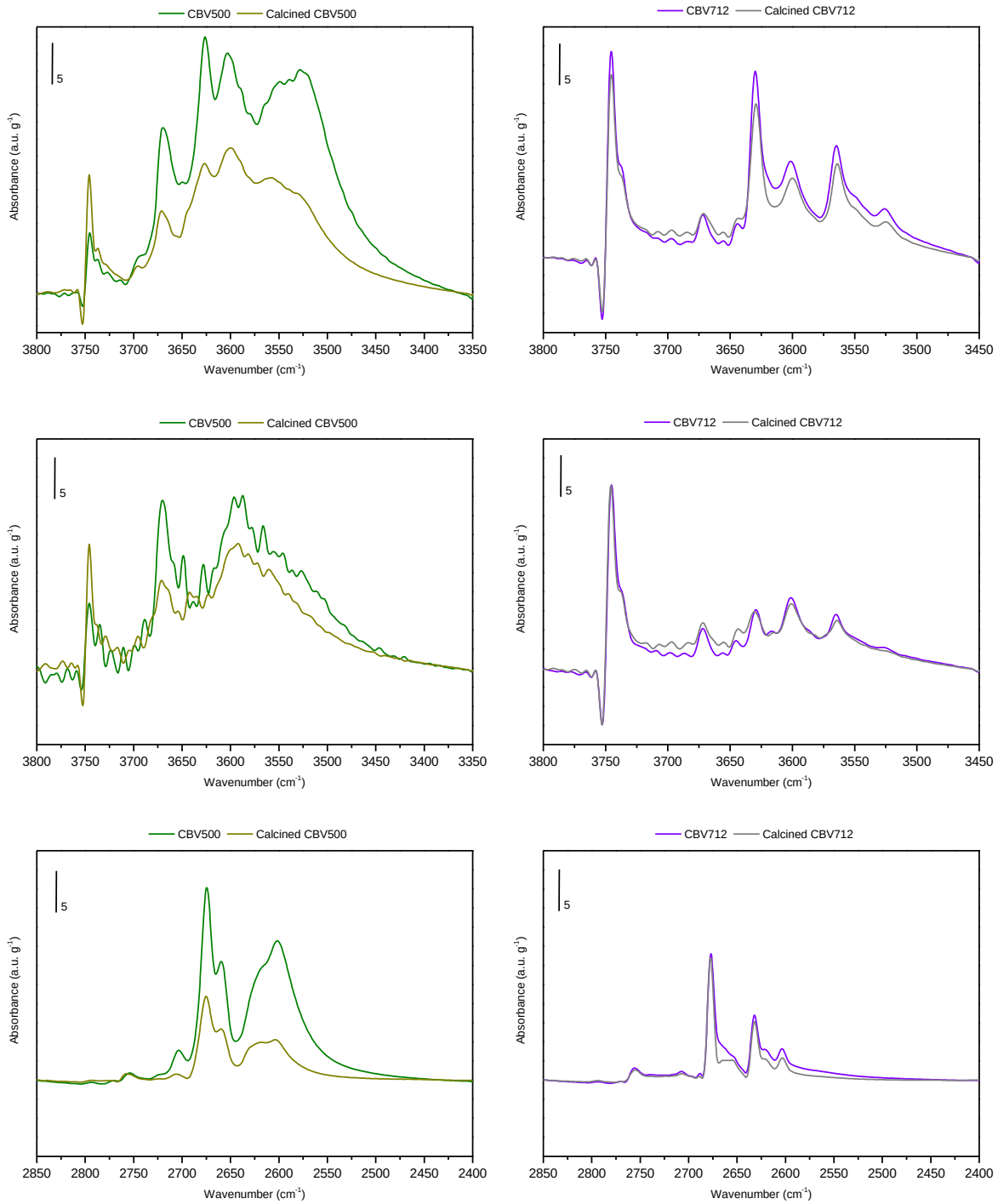

Figure 15 : Calcination effect on CBV500 (left) and CBV712 (right). Comparison between activated spectra (top) and spectra after 15 minutes contact for the hydroxyl region (center) and deuteroxyl region (bottom)

When comparing the OD/OH results for these samples, the calcined CBV500 shows a lower value than its parent zeolite (0,32 compared to 0,44), whereas the calcined CBV712 shows a higher value (0,55 opposed to 0,49). Concerning the first case, these results might be a consequence of pore

blocking, or to accessibility or diffusional constraints on calcined CBV500 due to its purely microporous structure. As for the second case, the ratio increases due to the loss of some of its weak acid sites.

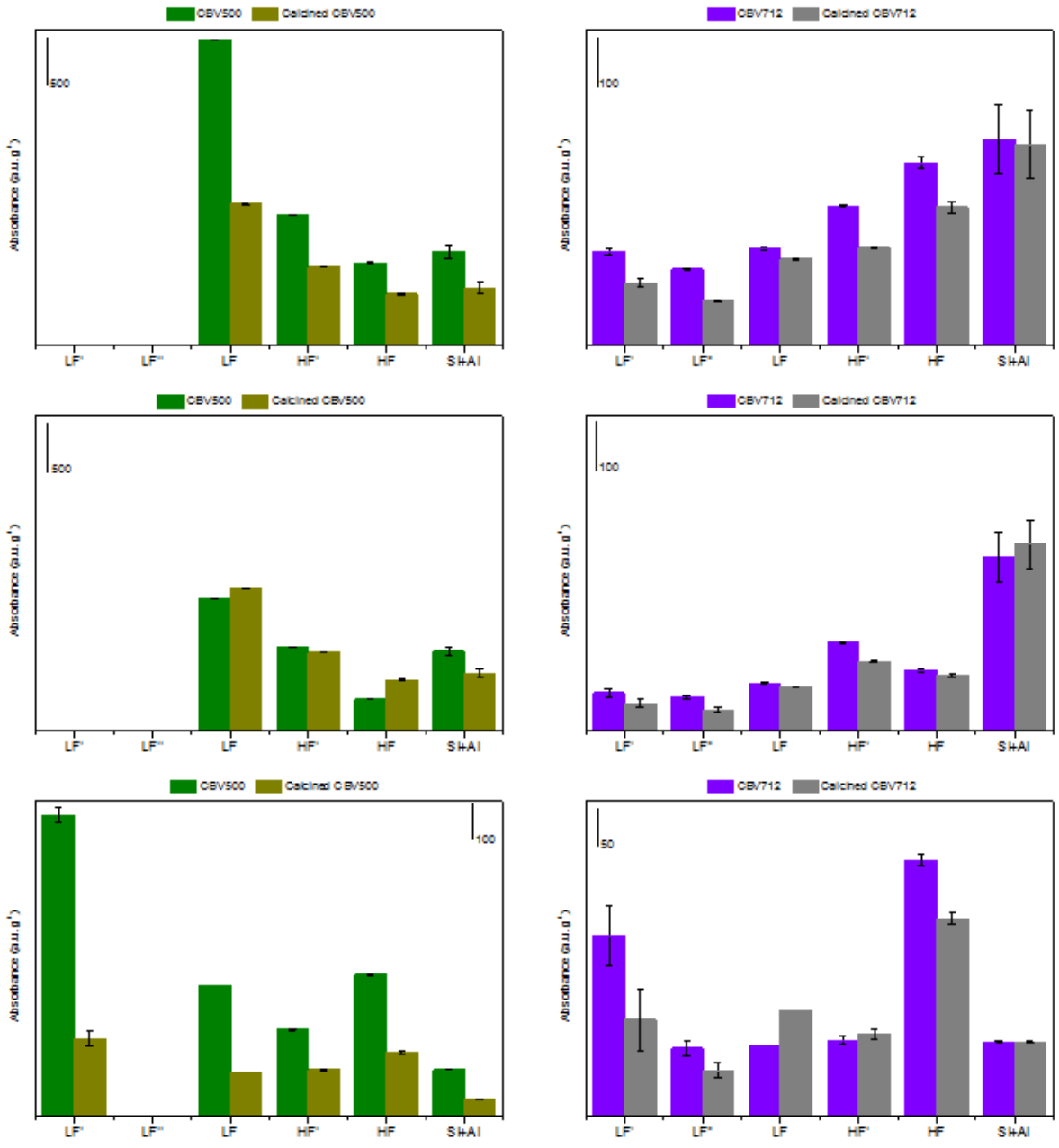

Figure 16 : Quantification of all acid sites found in CBV500 and calcined CBV500 (top) and in CBV712 and calcined CBV712 (bottom). Results for the hydroxyl region on the activated spectra (left) and after 15 minutes exchange (center). Results on the deuteroxyl region after 15 minutes exchange on the right

It can then be proven that calcination directly influences textural properties such as the specific area (see Table 4), the porosity volume and the pore size distribution, while indirectly affecting the activity, selectivity and stability of the catalyst.

5.2.4 Modification effect

CBV720 has been subjected to modification by two different procedures: conventional steaming (Steamed CBV720) and by acid treatment in liquid phase (Modified CBV720). Both samples were compared to each other and with the respective parent zeolite. The results can be consulted in Figure 17.

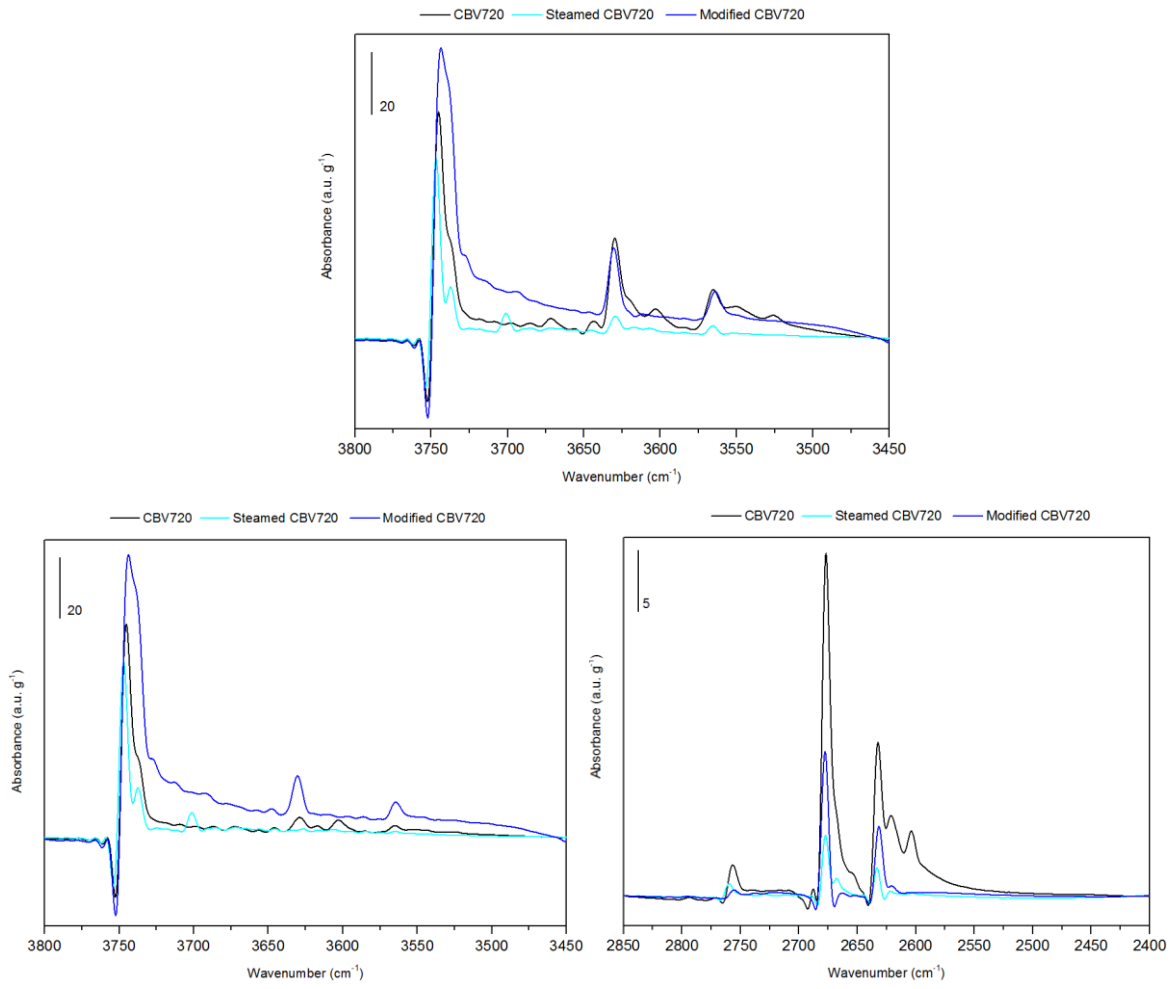

Figure 17 : Modified CBV720 by steaming or by acid treatment. Comparison between activated spectra (top) and spectra after 15 minutes contact for the hydroxyl region (bottom left) and deuteroxyl region (bottom right)

Most of the original acidity is removed when the parent zeolite is steamed. Just by looking at the activated spectra, one can easily spot the absence of the very defined bands seen on the parent

sample attributed to the high frequency and the low frequency acid sites. Specifically, the bands related to perturbed species are almost imperceptible in the resulting steamed spectra, whereas the HF and LF signal are present, but with a much lower intensity. It should be noted, as well, that there appears to be a new contribution at 3700 cm^{-1} that cannot be spotted in the parent zeolite. This new component could be assigned to OH oligomeric Al species. As well, even though there is a shoulder at 3738 cm^{-1} on the original sample, the ensuing steamed sample shows a much more defined shoulder at the same wavenumber, even if its overall intensity is lower.

When looking at the spectra after 15 minutes contact, it is easily concluded that almost all the available acid sites on both the steamed and the parent zeolite have undergone H/D exchange, except for the silanol groups (weakly acidic) and the contribution at 3700 cm^{-1} on the steamed sample. These conclusions can be further completed by looking at the deuteroxyl region of the spectra after 15 minutes contact with C_6D_6. In this case, the distinction between the different acid sites is much more straightforward, and it can even be observed that, in contrary to what could be taken from the activated spectra in the hydroxyl region, there is possibly a very short contribution of perturbed HF' acid sites in the steamed sample (evidenced by FSD treatment).

As hypothesized when comparing the spectra taken in the hydroxyl region for the activated samples and after 15 minutes contact, it is confirmed that the contribution at 3700 cm^{-1} does not undergo H/D exchange, as there is no observed band at the corresponding wavenumber for the deuteroxyl region (2740 cm^{-1}). As such, the oligomeric Al species should portray a very weakly or non-acidic behavior. Lastly, the silanol region is altered on the steamed sample, which reports two distinct maxima.

Now discussing on the Modified CBV720, one notices that this sample displays a very broad contribution between 3730 cm^{-1} and 3460 cm^{-1}. The short band found in the deuteroxyl spectra at 2620 cm^{-1} can be attributed to LF'OH sites. The presence of this band could not be envisioned when looking at the hydroxyl spectra, masked by the broad effect of the bands in this region.

Despite the intensity of the HFOH and the LFOH being somewhat kept after acid treatment, a part of these sites does not exchange after 15 minutes, whereas an extended level of exchange can be seen for the parent zeolite. In fact, the HFOD and LFOD bands on the modified sample show around half of the intensity of the corresponding bands on CBV720.

The quantitative results are in line with what has been previously discussed qualitatively. For instance, when concerning the activated spectra, it can be concluded that both modification procedures (steaming and acid treatment) removed the perturbed acid sites. Despite the low content of acid sites on the steamed sample, it seems that they undergo almost total exchange, judging by the almost imperceptible bands remaining after 15 minutes exchange.

Thus, when calculating the OD/OH ratio, the steamed sample shows a much higher value (~1) than what is obtained for the modified sample and for the parent zeolite (respectively, 0,45 and 0,88), translating into a higher proportion of strong acid sites that can easily undergo exchange.

This is mainly due to the fact that these two modification procedures unfold in different ways. The modification by acid treatment forms silanol nests, seen by the noticeable band on the quantitative results concerning the silanol sites and by the broad band found on the spectra for the corresponding wavenumbers. The dealumination is possibly much more selective towards the sites of enhanced acidity than what is obtained by steaming. In fact, this removal also occurs on the steamed sample, but the removal of the overall acidity is much more extensive and not just limited to those groups.

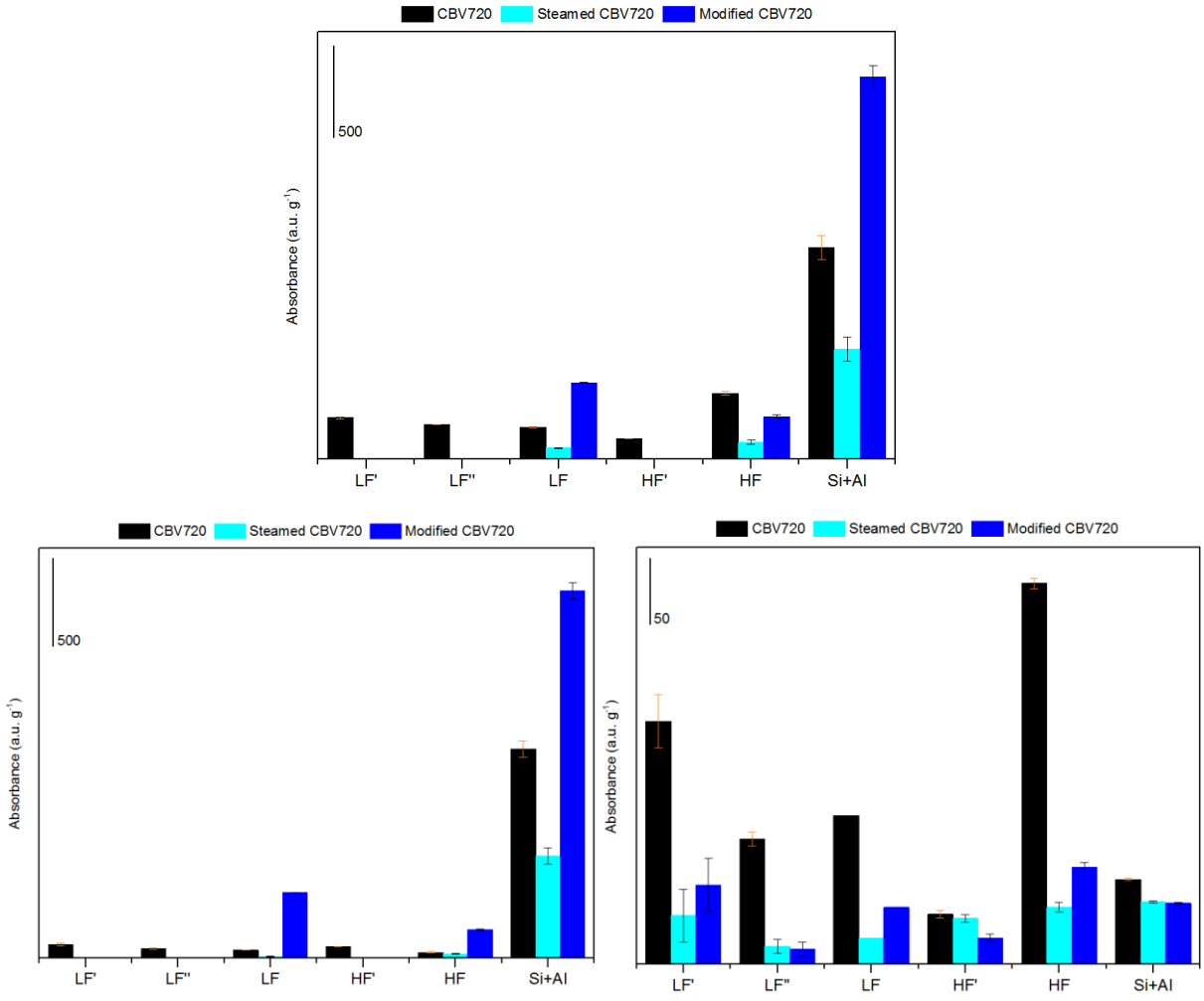

Figure 18 : Quantification of all acid sites found in CBV720 and its modified versions by steaming and by acid treatment. Results for the hydroxyl region on the activated spectra (left) and after 15 minutes exchange (center). Results on the deuteroxyl region after 15 minutes exchange on the right

5.2.5 Shaping effect

The effect of shaping a zeolite has also been studied in the present report. In this section, both the parent CBV720 zeolite and its modified version by acid treatment were mixed with an alumina binder (ex boehmite) and subjected to analysis.

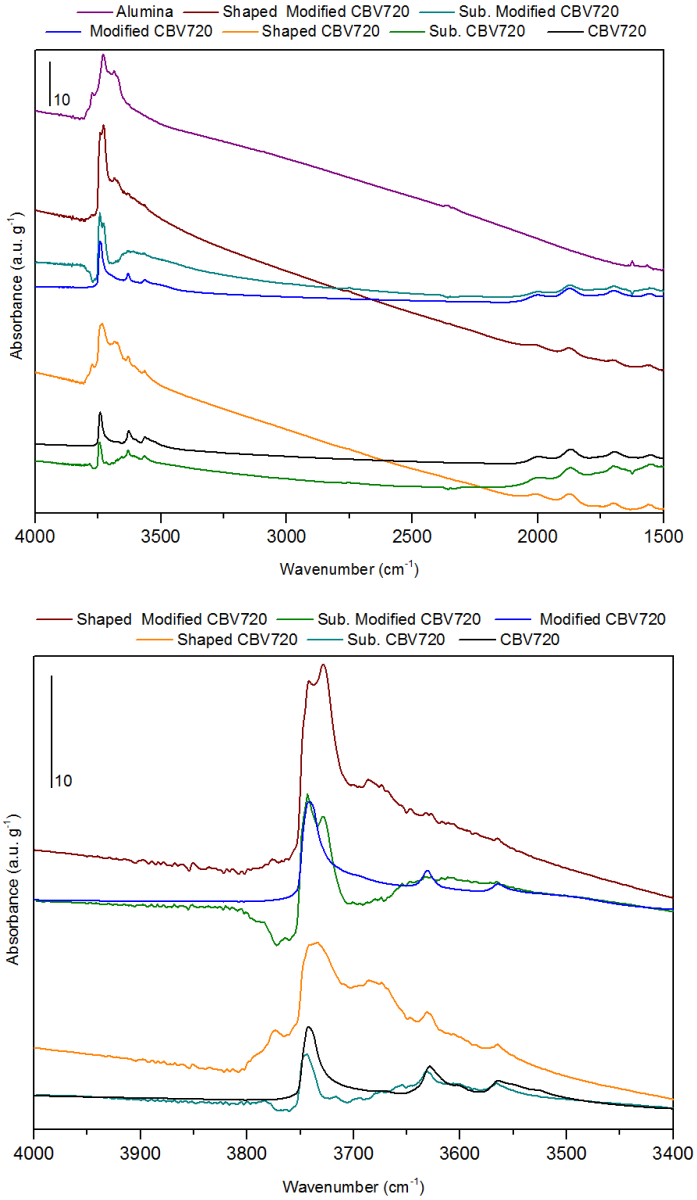

Figure 19 : Shaping effect on CBV720. Comparison between alumina activated spectrum (top) and activated spectra of CBV720 and modified CBV720 before and after shaping. Subtracted spectra are also included for both cases. On the bottom is the zoomed hydroxyl region of the same spectra

Figure 19 shows all the activated spectra relevant for discussion. The spectra of the activated alumina binder can be found right at the top. Following, are the spectra concerning the shaped and the non-shaped CBV720 (multiplied by the dilution factor), as well as the spectrum resulting from the subtraction of the alumina binder to the shaped zeolite. At the bottom, the equivalent spectra as the previously mentioned for the modified sample are included for the parent zeolite.

Starting out by the results obtained for the parent zeolite, striking differences in the aspect of the activated spectra can be distinguished after shaping, mostly due to the contribution of the alumina binder. Subtracting this contribution to the shaped spectrum illustrates the zeolite content in the shaped sample (spectrum at the bottom). The subtracted and the original spectra are not superposable, which leads to the conclusion that the shaping step induces modifications on the zeolite, even if the zeolitic content is kept approximately constant (as concluded by comparing the bands at ~1800cm^{-1}, concerning the T-O-T vibration modes of the zeolite).

In fact, when shifting the attention to the bottom spectra (zoom of the top part mentioned above) of Figure 19, a different distribution of the acid sites is clearly observed. Part of the aluminols have been consumed (as seen by the negative signal found at ~3768 cm^{-1} and 3720 cm^{-1}), as well as a small fraction of the HFOH, and all contributions on the LF region. It seems, as well, that the bands for LF''OH and LF'OH are no longer distinguishable.

As for the activated spectrum of the shaped modified sample, its profile is closer to what would be obtained for a non-shaped zeolite, apart from the new band that can be observed at ~3730 cm^{-1}, not found on the non-modified shaped zeolite.

By comparison between the subtracted and the original spectra of the modified zeolite, an even more pronounced consumption of the aluminols can be reported. However, differently from what found on the parent zeolite, the bands attributed to both the HFOH and LFOH groups are difficult to visualize and replaced by a broad band at ~3650 cm^{-1}. The most interesting feature falls on the new band at 3730 cm^{-1}, thus concluding that shaping of the modified sample created a new OH species and a distinct distribution of the acid sites. The extent of the shaping induced alterations is much more prominent on this sample than on the shaped non modified CBV720.

It is also interesting to check how this new contribution interacts with C_6D_6. When looking at the results after 15 minutes exchange at room temperature (see bottom portion of Figure 20), the new contribution is clearly exchanged, evidenced in the OD region at ~2750cm^{-1}. In fact, when following the exchange as a function of the contact time, this species is one of the first to start exchanging and to reach an equilibrium, proving to display an acidity close to that of hydroxyl acid sites. This exchange is also part of a set of broad bands appearing on higher wavenumbers, not found on the non-shaped zeolite.

The observations on the different acid sites found on the activated spectra are confirmed in the deuteroxyl region. It should be noted that the differences on these bands are much more pronounced for these samples than for the modified CBV720 before and after shaping.

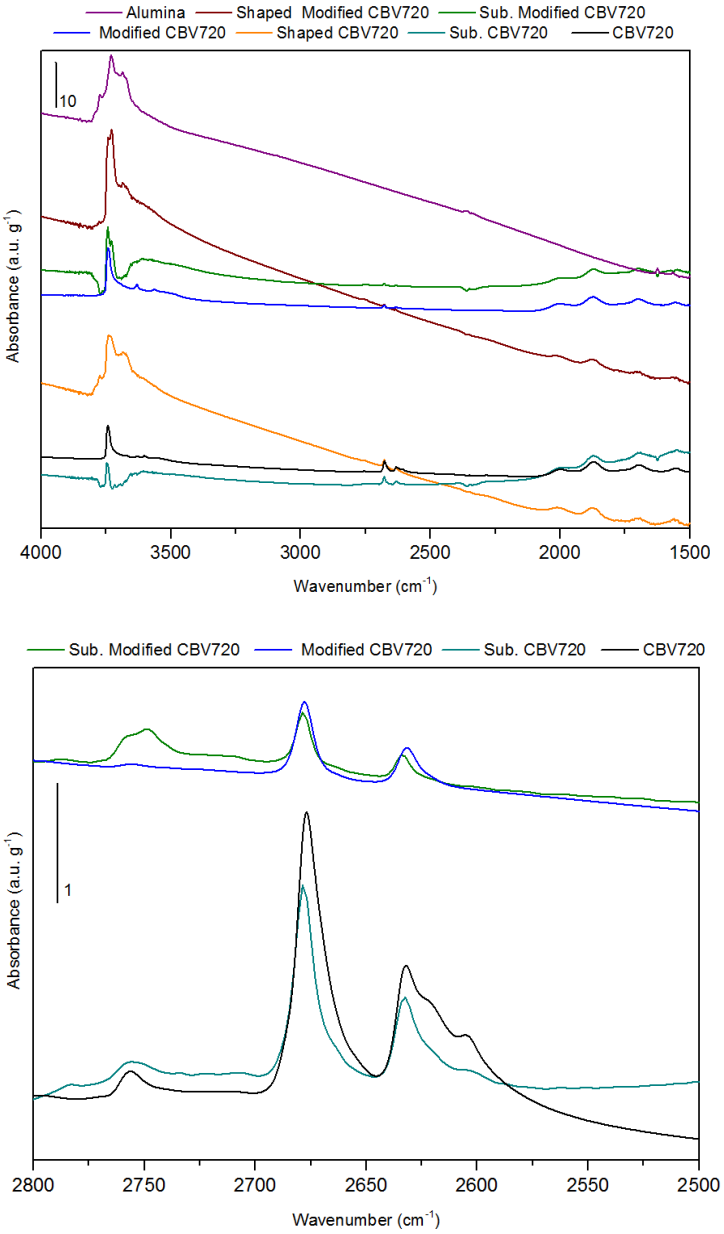

Figure 20 : Shaping effect on CBV720. Comparison between alumina activated spectrum (top) and spectra of CBV720 and modified CBV720 before and after shaping after 15 minutes exchange at room temperature. Subtracted spectra are also included for both cases. On the bottom is the zoomed deuteroxyl region of the same spectra

6 Conclusions

Different techniques have been developed in order to study and characterize acid sites found in zeolites and other catalysts. However, a recurring problem with these relates to the impossibility of discriminating between each type of acid sites, only providing an estimation of the bulk acidity of the samples.

In line with the results that have previously been discussed in this section, employing C_6D_6 as a probe molecule can be used to simultaneously characterize most of the acid sites found on zeolites. It also allows to follow the H/D exchange as a function of the exchange time for all different types of sites, screening their accessibility and their acidic strength. Additionally, it proves to be sensitive enough to study the influence of distinct parameters on the acidity, such as the distribution of acid sites according to the Si/Al ratio, and the effects of modification treatments, namely calcination, steaming or acid treatment or, even, the effect induced by the shaping step.

In fact, the shaping effect should be studied in further detail. Despite the experiments having been repeated twice with the same findings, more experiments should be performed to determine the nature and origin of the new contribution found on the shaped modified CBV720.

As a closing note, it proves to be a reliable technique, judging by the reproducibility of the obtained results (see Appendix A).

(This page was intentionally left in blank)

7 Future works and perspectives

Following up the work that has been previously disclosed, a quite substantial amount of information can still be obtained by employing the developed technique.

For instance, it would be interesting to test this methodology with other types of probe molecules. In fact, a bulkier molecule, deuterated trimethylbenzene (1,3,5-Trimethylbenzene-d_{12}, *Sigma Aldrich*, 98 atom % D), has also been tested for zeolitic samples in the present study, namely for CBV500, CBV720 and the modified CBV720. By studying these samples, it was aimed to determine how the exchange could be affected by spatial and diffusional constraints, namely concerning the microporous profile of CBV500.

It was concluded that the experimental procedure had to be modified when using this probe molecule, as the removal of the physisorbed species inside the setup would not occur at room temperature, regardless of the duration of the evacuation step. Due to this, the first contacts at room temperature were performed in the same manner as previously addressed for C_6D_6, but the first information on the exchange was obtained only after evacuation at 150ºC. As the temperature was increased, a dual effect might have been at play: the evacuation of the physisorbed species and the enhancement of the exchange by less acidic sites.

Considering the above, only the results obtained after 30 minutes exchange at higher temperature have been compared to the equivalent results when using C_6D_6. It should also be noted that instead of the introduction of 20 mbar of probe molecule in each contact, a fixed value of 3 mbar has been used, due to the impossibility of increasing the vapor pressure to higher values when using deuterated trimethylbenzene. The comparison between the obtained results for each probe molecule can be seen in Figure 21.

Generally, not many differences can be found between the amount of acid sites probed by C_6D_6 and by deuterated trimethylbenzene. In fact, an increase in the exchange of the enhanced HF' sites can be discerned for CBV720 and its modified version when using this bulkier molecule, as well as LF, LF'' and LF' on the modified CBV720. Thus, the accessibility of the acid sites remains the same, regardless of the probe molecule that was used. The most striking differences are found for CBV500, where the quantification of the acid sites is lower when using deuterated trimethylbenzene instead of C_6D_6, possibly due to its microporous structure.

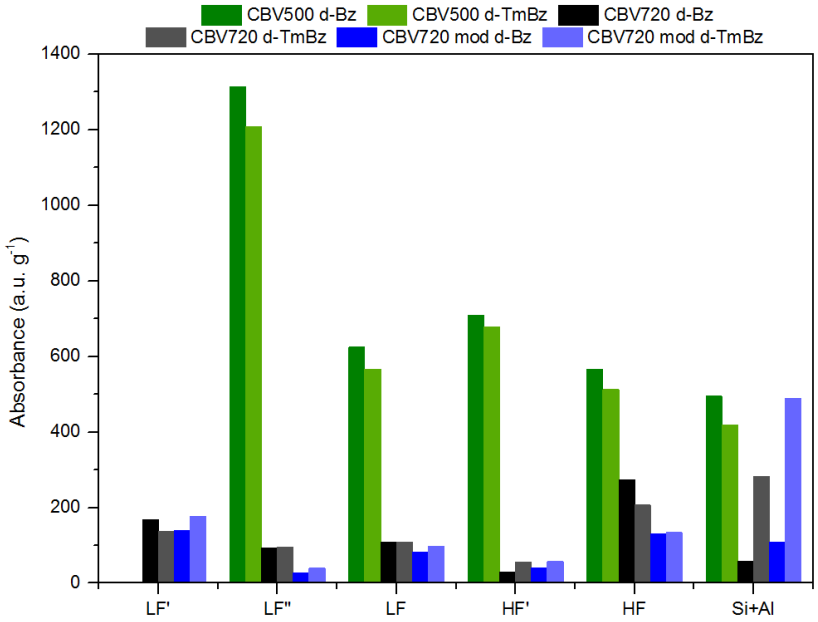

Figure 21 : Quantification of acid sites for CBV500, CBV720 and modified CBV720 in the deuteroxyl region, when using deuterated benzene (d-Bz) and deuterated trimethylbenzene (d-TmBz) as probe molecule

A future work of interest would be to test an even bulkier molecule, such as triisopropylbenzene. However, the deuterated molecule is not available, so the experimental procedure would have to be modified. One way would be to perform full H/D exchange using C_6D_6, and then make the sample contact with triisopropylbenzene, in order to follow the D/H exchange, obtaining information on the accessibility of the sites.

Another possibility would be to test different experimental procedures for the same probe molecule. Perhaps, the most interesting would be to increase the temperature for a fixed contact time, opposite of the experimental procedure employed in the present report. This way, one would be studying the acid strength and availability of the sites (as the increase in temperature will enable the diffusion of the probe molecule, and the contact with more confined acid sites). Information on the temperature at which the total H/D exchange is reached would also be obtained.

The effect of the vapor pressure should also be investigated, as this parameter regulates the amount of gas phase C_6D_6 introduced in the setup. This way, it would be possible to determine, for instance, when saturation of the sites is reached. An experiment on CBV720 where 3 mbar of C_6D_6 has been introduced in each contact was also performed. The comparison between the results collected in this case and when using 20 mbar is found in Figure 22.

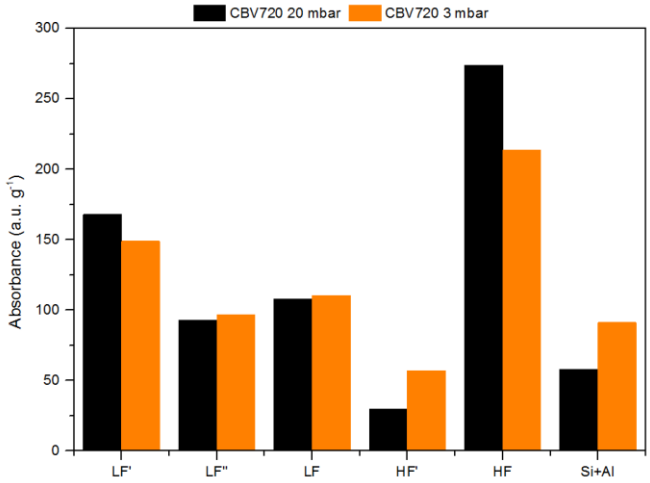

Figure 22 : Quantification of acid sites on CBV720, using a vapor pressure of 20 mbar and 3 mbar

It appears that the extent of exchange when using 20 mbar and 3 mbar is similar. However, further studies are necessary in order to validate the significance of these results.

(This page was intentionally left in blank)

8 References

[1] Poduval D. G. *On the role of acidity in amorphous silica-alumina based catalysts*. Technische Universiteit Eindhoven, 2011, 177 p.

[2] Beale A.M., Gao F., Lezcano-Gonzalez I., Peden C.H. F., Szanyi J. Recent advances in automotive catalysis for NOx emission control by small-pore microporous materials, *Chemical Society reviews*, 2015, 44, 20, 7371-7405. DOI: 10.1039/c5cs00108k.

[3] Borfecchia E., Beato P., Svelle S., Olsbye U., Lamberti C., Bordiga S. Cu-CHA - a model system for applied selective redox catalysis, *Chemical Society reviews*, 2018, 47, 22, 8097-8133. DOI: 10.1039/c8cs00373d.

[4] Kerkeni B., Berthout D., Berthomieu D., Doronkin D.E., Casapu M., Grunwaldt J.-D., Chizallet C. Copper Coordination to Water and Ammonia in Cu II -Exchanged SSZ-13 : Atomistic Insights from DFT Calculations and in Situ XAS Experiments, *The Journal of Physical Chemistry C*, 2018, 122, 29, 16741-16755. DOI: 10.1021/acs.jpcc.8b03572.

[5] Priya S.V., Ohnishi T., Shimada Y., Kubota Y., Masuda T., Nakasaka Y., Matsukata M., Itabashi K., Okubo T., Sano T., Tsunoji N., Yokoi T., Ogura M. A Collective Case Screening of the Zeolites made in Japan for High Performance NH_3-SCR of NOx, *Bulletin of the Chemical Society of Japan*, 2018, 91, 3, 355-361. DOI: 10.1246/bcsj.20170352.

[6] Figueiredo J. L., Ribeiro F. R., Lemos F., Orfão J. J. M. *Catálise heterogénea*. Fundação Calouste Gulbenkian, Lisboa, 2015, 352 p.

[7] Malicki N. *Développement des spectroscopies RMN et Infra-rouge de molécules adsorbées pour l'étude de zéolithes partiellement échangées avec des cations,* 173 p.

[8] Phung T.K., Busca G. On the Lewis acidity of protonic zeolites, *Applied Catalysis A: General*, 2015, 504, 151-157. DOI: 10.1016/j.apcata.2014.11.031.

[9] Sandoval-Díaz L.E., González-Amaya J.A, Trujillo C.A. General aspects of zeolite acidity characterization, *Microporous and Mesoporous Materials*, 2015, 215, 229-243. DOI: 10.1016/j.micromeso.2015.04.038.

[10] Hadjiivanov K. *Identification and Characterization of Surface Hydroxyl Groups by Infrared Spectroscopy*. Elsevier, 2014, 220 p.

[11] Speight J. G. *The Refinery of the Future*. Elsevier Science, 2010.

[12] Chester A.W. Zeolite Characterization and Catalysis: A Tutorial, Springer 2009, 373 p.

[13] Vazhnova T., Lukyanov D.B. Fourier self-deconvolution of the IR spectra as a tool for investigation of distinct functional groups in porous materials : Brønsted acid sites in zeolites, *Analytical chemistry*, 2013, 85, 23, 11291-11296. DOI: 10.1021/ac4020337.

[14] Che M., Vedrine J. C. *Characterization of solid materials and heterogeneous catalysts : From structure to surface reactivity*. Wiley-VCH, Weinheim, 2012, 48 p.

[15] Derouane E.G., Védrine J.C., Pinto R.R., Borges P.M., Costa L., Lemos M.A.N.D.A., Lemos F., Ribeiro F.R. The Acidity of Zeolites : Concepts, Measurements and Relation to Catalysis: A Review on Experimental and Theoretical Methods for the Study of Zeolite Acidity, *Catalysis Reviews*, 2013, 55, 4, 454-515. DOI: 10.1080/01614940.2013.822266.

[16] Kondo J.N., Nishitani R., Yoda E., Yokoi T., Tatsumi T., Domen K. A comparative IR characterization of acidic sites on HY zeolite by pyridine and CO probes with silica-alumina and γ-alumina references, *Physical chemistry chemical physics : PCCP*, 2010, 12, 37, 11576-11586. DOI: 10.1039/c0cp00203h.

[17] Ward John W. The nature of active sites on zeolites : I. The decationated Y zeolite, *Journal of Catalysis*, 1967, 9, 3, 225-236. DOI: 10.1016/0021-9517(67)90248-5.

[18] Jacobs P. U.J.B. Infrared study of deep-bed calcined NH_4Y zeolites, *Journal of Catalysis*, 1971, 22, 2, 193-203. DOI: 10.1016/0021-9517(71)90185-0.

[19] Maxwell I. E. Zeolite catalysis in hydroprocessing technology, *Catalysis Today*, 1987, 1, 4, 385-413. DOI: 10.1016/0920-5861(87)80006-8.

[20] Karge H. G., Weitkamp J., Baerlocher C., Bennett J. M., Depmeier W., Fitch A. N., Jobic H., van Koningsveld H., Meier W. M., Pfenninger A., Terasaki O. *Structures and Structure Determination*. Springer Berlin Heidelberg, Berlin, Heidelberg, 1999.

[21] Verboekend D., Nuttens N., Locus R., van Aelst J., Verolme P., Groen J.C., Pérez-Ramírez J., Sels B.F. Synthesis, characterisation, and catalytic evaluation of hierarchical faujasite zeolites : Milestones, challenges, and future directions, *Chemical Society reviews*, 2016, 45, 12, 3331-3352. DOI: 10.1039/c5cs00520e.

[22] Scherzer J., Bass Jonathan L. Infrared spectra of ultrastable zeolites derived from type Y zeolites, *Journal of Catalysis*, 1973, 28, 1, 101-115. DOI: 10.1016/0021-9517(73)90184-X.

[23] Cairon O. Impacts of composition and post-treatment on the Bronsted acidity of steam-treated faujasite : Insights from FTIR spectroscopy, *Chemphyschem : a European journal of chemical physics and physical chemistry*, 2013, 14, 1, 244-251. DOI: 10.1002/cphc.201200568.

[24] Xue N., Vjunov A., Schallmoser S., Fulton J.L., Sanchez-Sanchez M., Hu J.Z., Mei D., Lercher J.A. Hydrolysis of zeolite framework aluminum and its impact on acid catalyzed alkane reactions, *Journal of Catalysis*, 2018, 365, 359-366. DOI: 10.1016/j.jcat.2018.07.015.

[25] Aramburo L.R., Karwacki L., Cubillas P., Asahina S., Winter D.A. M. de, Drury M.R., Buurmans I.L. C., Stavitski E., Mores D., Daturi M., Bazin P., Dumas P., Thibault Starzyk F., Post J.A., Anderson M.W., Terasaki O., Weckhuysen B.M. The porosity, acidity, and reactivity of dealuminated zeolite ZSM-5 at the single particle level : The influence of the zeolite architecture, *Chemistry (Weinheim an der Bergstrasse, Germany)*, 2011, 17, 49, 13773-13781. DOI: 10.1002/chem.201101361.

[26] Dufresne P., Bigeard P.H., Billon A. New developments in hydrocracking : Low pressure high-conversion hydrocracking, *Catalysis Today*, 1987, 1, 4, 367-384. DOI: 10.1016/0920-5861(87)80005-6.

[27] Jiang J., Dong Z., Chen H., Sun J., Yang C., Cao F. The Effect of Additional Zeolites in Amorphous Silica–Alumina Supports on Hydrocracking of Semirefined Paraffinic Wax, *Energy & Fuels*, 2013, 27, 2, 1035-1039. DOI: 10.1021/ef3013807.

[28] Karge H.G., Geidel E. Vibrational Spectroscopy, in *Molecular sieves* : *Science and technology.* Éd. H. G. Karge, J. Weitkamp. Springer-Verlag, Berlin, New York, 1998-, 1-200.

[29] Layman K.A., Ivey M.M., Hemminger J.C. Pyridine Adsorption and Acid/Base Complex Formation on Ultrathin Films of γ-Al_2O_3 on NiAl(100), *The Journal of Physical Chemistry B*, 2003, 107, 33, 8538-8546. DOI: 10.1021/jp030046p.

[30] Bourne K.H., Cannings F.R., Pitkethly R.C. Structure and properties of acid sites in a mixed-oxide system. I. Synthesis and infrared characterization, *The Journal of Physical Chemistry*, 1970, 74, 10, 2197-2205. DOI: 10.1021/j100909a028.

[31] Hensen E.J.M., Poduval D.G., Degirmenci V., Ligthart D.A.J. M., Chen W., Maugé F., Rigutto M.S., van Veen J.R. Acidity Characterization of Amorphous Silica–Alumina, *The Journal of Physical Chemistry C*, 2012, 116, 40, 21416-21429. DOI: 10.1021/jp309182f.

[32] Derouane E.G., Chang C.D. Confinement effects in the adsorption of simple bases by zeolites, *Microporous and Mesoporous Materials*, 2000, 35-36, 425-433.

[33] Kotrel S., Lunsford J.H., Knözinger H. Characterizing Zeolite Acidity by Spectroscopic and Catalytic Means : A Comparison, *The Journal of Physical Chemistry B*, 2001, 105, 18, 3917-3921. DOI: 10.1021/jp002161v.

[34] Kauppinen J.K., Moffatt D.J., Mantsch H.H., Cameron D.G. Fourier transforms in the computation of self-deconvoluted and first-order derivative spectra of overlapped band contours, *Analytical Chemistry*, 1981, 53, 9, 1454-1457. DOI: 10.1021/ac00232a034.

[35] Hensen E.J. M., Poduval D.G., Ligthart D.A. J. M., van Veen J.A. R., Rigutto M.S. Quantification of Strong Brønsted Acid Sites in Aluminosilicates, *The Journal of Physical Chemistry C*, 2010, 114, 18, 8363-8374. DOI: 10.1021/jp9106348.

Appendix

A - Reproducibility tests on zeolites

Reproducibility tests have been performed on two batches of CBV720 in order to verify the accuracy of the method.

1. CBV720

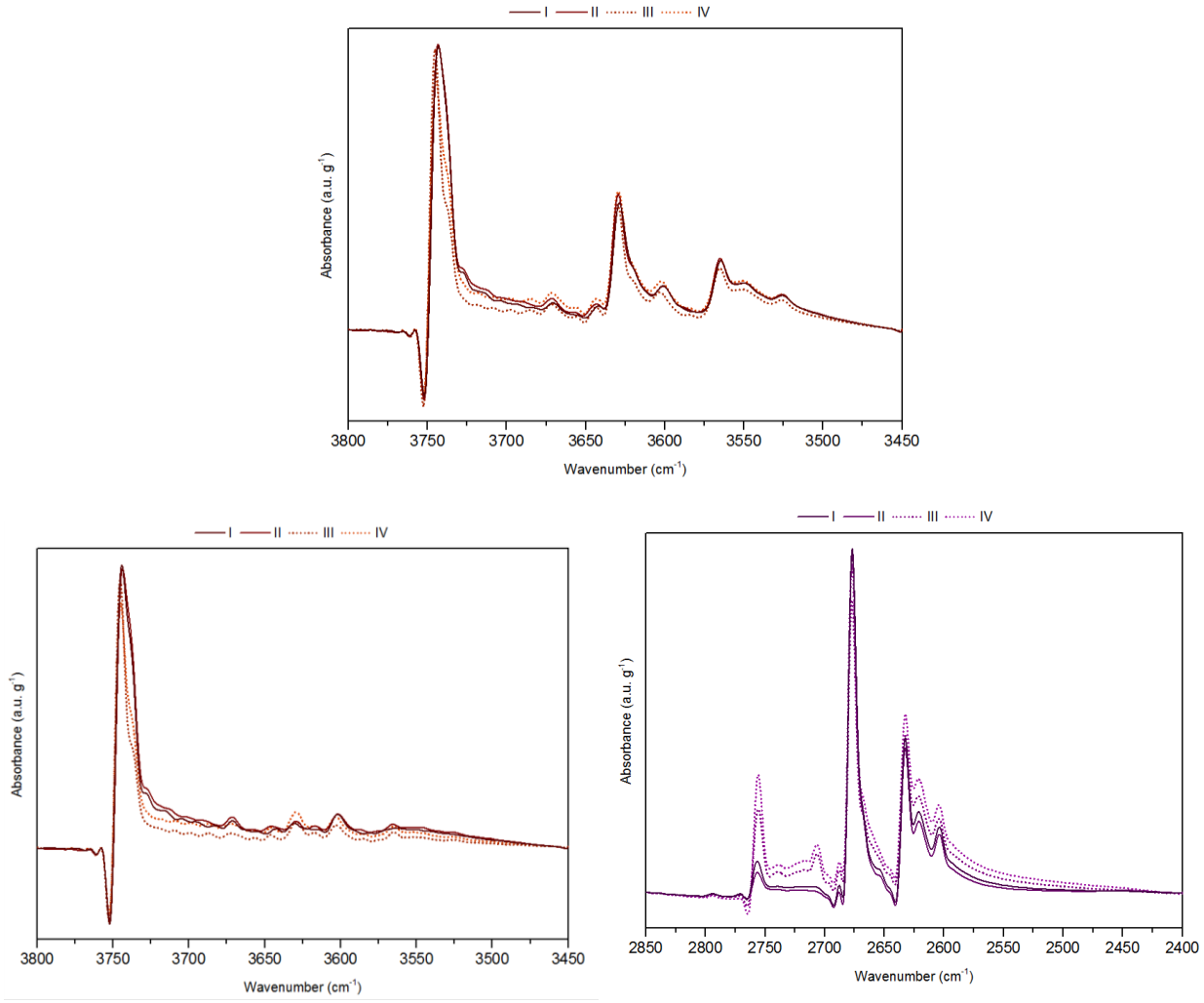

Figure 23: CBV720 spectra for four different experiments. Activated spectra (top) and spectra after 15 minutes exchange (bottom left) for the hydroxyl region, spectra after 15 minutes exchange for the deuteroxyl region (bottom right)

The dotted lines in Figure 23 correspond to experiments that have been discarded due to a different evolution of H/D exchange. Quantitative results and standard deviation calculated using the four spectra and the remaining two are disclosed in Table 7 and Figure 24. Standard deviation used in the report corresponds to the latter case (Standard deviation* on Table 7).

Table 7 : Quantification of acid sites by Direct Integration on four samples of CBV720

	CBV720	**I**	**II**	**III**	**IV**	**Standard deviation**	**Standard deviation ***
Activated Spectra (Hydroxyl Region)	**LF'**	228	237	200	205	18	6
	LF''	191	192	169	190	11	1
	LF	176	172	152	165	11	3
	HF'	113	112	97	103	8	1
	HF	363	378	348	378	14	11
	Si+Al	1165	1257	886	1006	165	65
15 minutes contact with C_6D_6 (Hydroxyl Region)	**LF'**	78	89	33	35	28	8
	LF''	56	61	29	36	19	5
	LF	47	46	27	33	14	1
	HF'	67	66	48	53	6	1
	HF	34	29	60	69	38	2
	Si+Al	1199	1265	798	934	193	45
15 minutes contact with C_6D_6 (Deuteroxyl Region)	**LF'**	175	148	152	192	21	18
	LF''	90	83	97	108	11	5
	LF	107	107	107	117	5	0
	HF'	36	40	36	38	2	2
	HF	274	279	221	243	27	1
	Si+Al	61	60	121	165	51	2

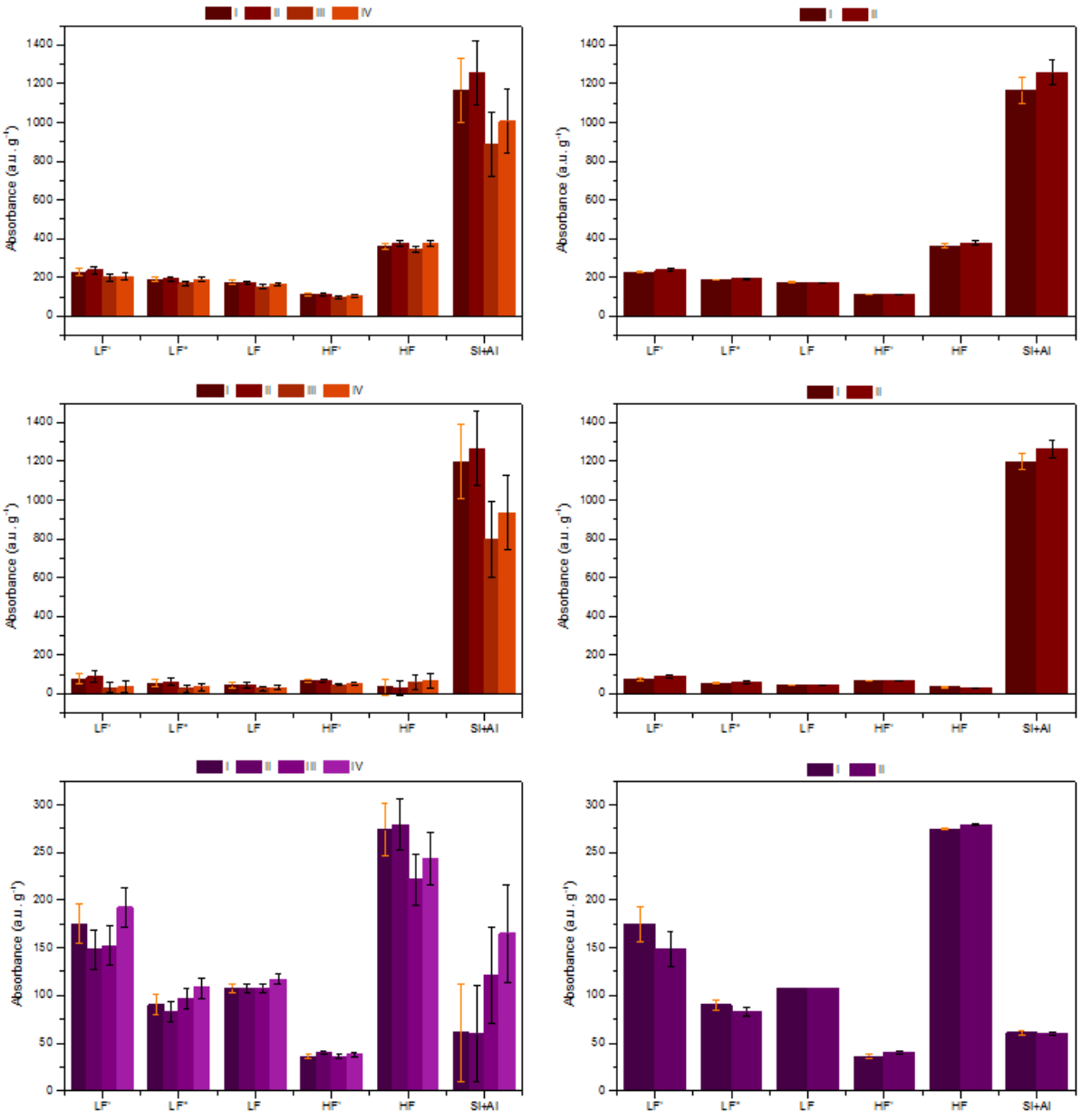

Figure 24: Acid sites quantification and standard deviation for CBV720. Used results on the right

2. CBV720 2nd batch

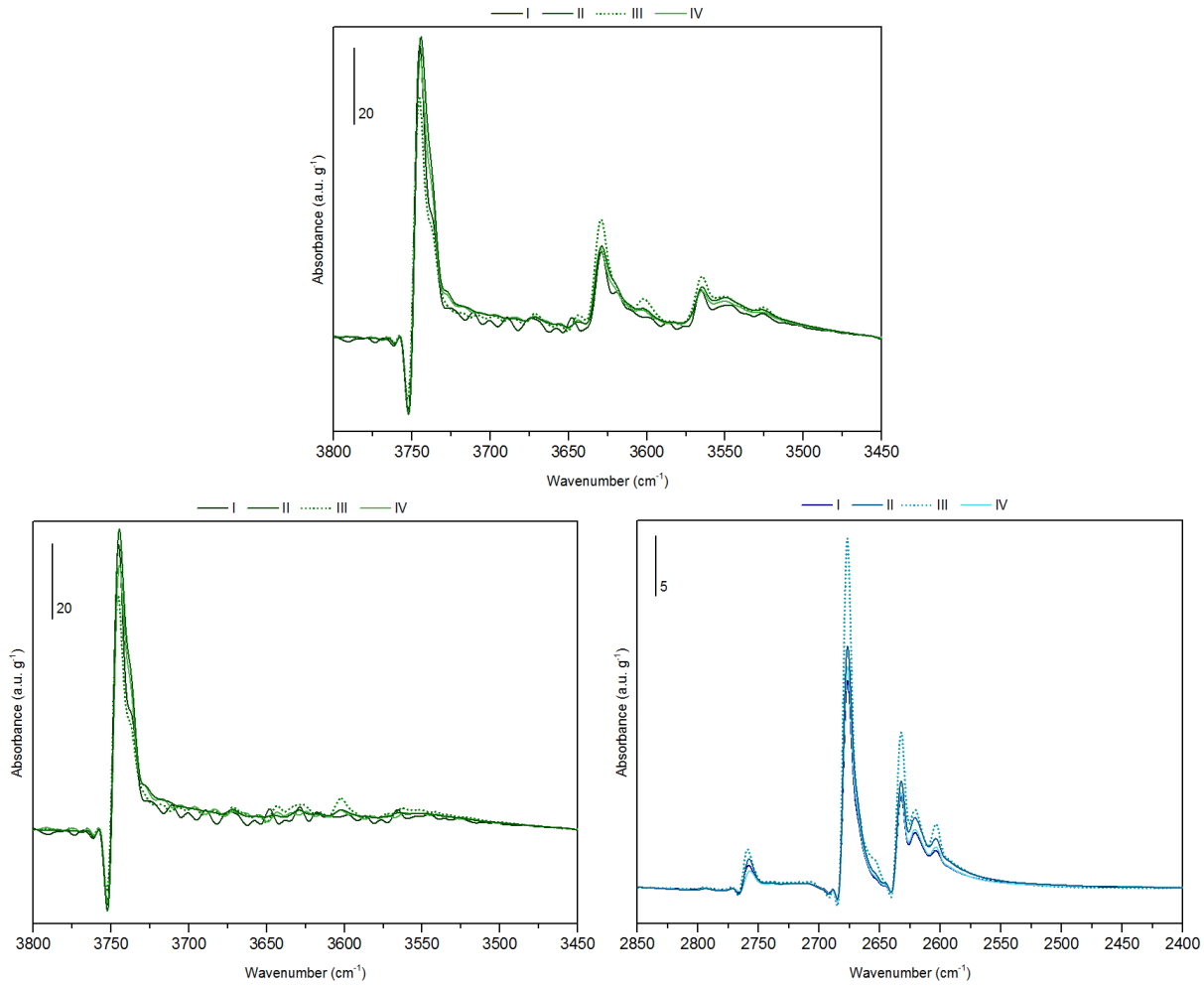

Figure 25: CBV720 2nd batch spectra for four different experiments. Activated spectra (top) and spectra after 15 minutes exchange (bottom left) for the hydroxyl region, spectra after 15 minutes exchange for the deuteroxyl region (bottom right)

The dotted line in Figure 25 corresponds to a discarded experiment, as it showed a different H/D exchange evolution. Quantitative results (Figure 26) and standard deviation calculated using the four spectra and the remaining three (Standard deviation* on Table 8) are disclosed below.

Table 8 : Quantification of acid sites by Direct Integration on four samples of CBV720 2nd batch

	CBV720	I	II	III	IV	Standard deviation	Standard deviation *
Activated Spectra (Hydroxyl Region)	**LF'**	210	267	180	182	41	17
	LF''	175	211	148	159	28	14
	LF	134	221	116	120	49	9
	HF'	77	175	75	71	50	3
	HF	302	453	281	284	83	11
	Si+Al	1152	1060	988	1078	67	82
15 minutes contact with C_6D_6 (Hydroxyl Region)	**LF'**	72	136	70	59	35	7
	LF''	53	102	51	48	26	3
	LF	40	105	37	30	35	5
	HF'	40	127	40	26	46	8
	HF	33	145	47	17	58	15
	Si+Al	1151	1054	961	1015	80	98
15 minutes contact with C_6D_6 (Deuteroxyl Region)	**LF'**	168	139	206	147	30	15
	LF''	86	71	101	76	13	8
	LF	82	70	119	75	22	6
	HF'	40	34	65	41	14	4
	HF	228	194	297	208	46	17
	Si+Al	77	74	113	77	19	2

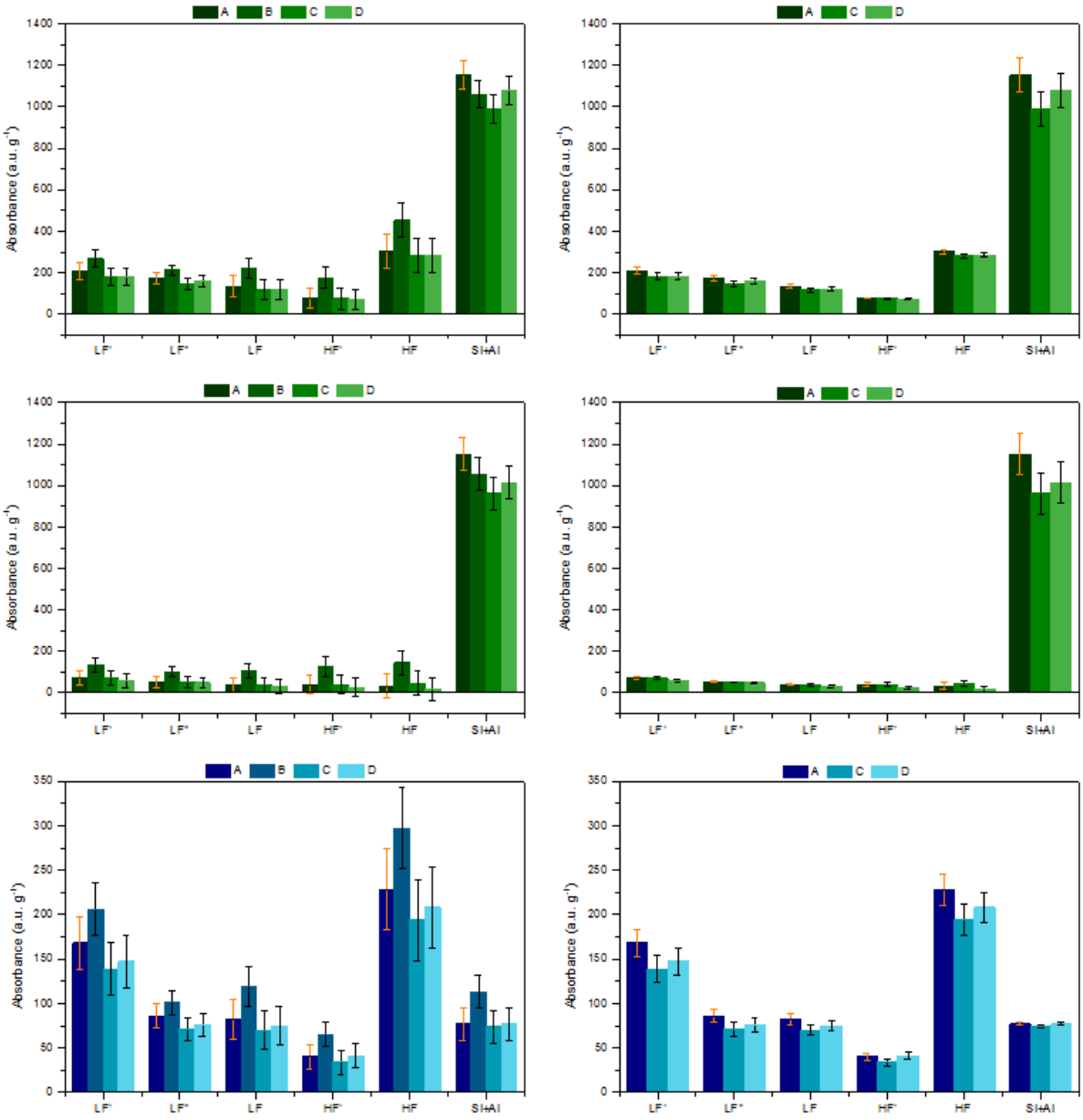

Figure 26 : Acid sites quantification and standard deviation for CBV720 2nd batch

B - Direct Integration on zeolites

The quantification of the different acid sites on the zeolites was obtained by Direct Integration of the FSD treated spectra on the *OMNIC* software. The first step was to take the same limits of integration for all samples and choose a baseline as straight as possible. Two different baselines were used, one for the silanol and aluminol groups, and another comprising the Brønsted acid sites. An example of what was performed on all samples can be consulted in Figure 27 and Figure 28 for the hydroxyl and for the deuteroxyl region, respectively.

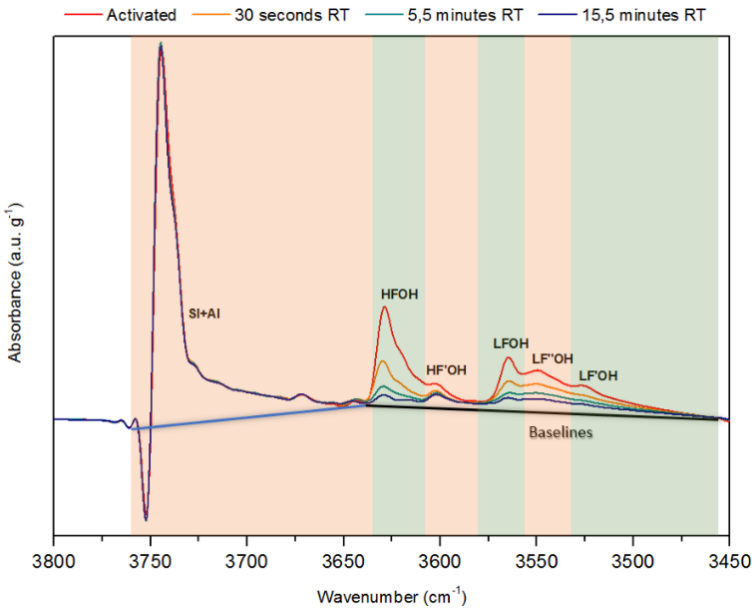

Figure 27: Direct integration on the hydroxyl region of CBV720

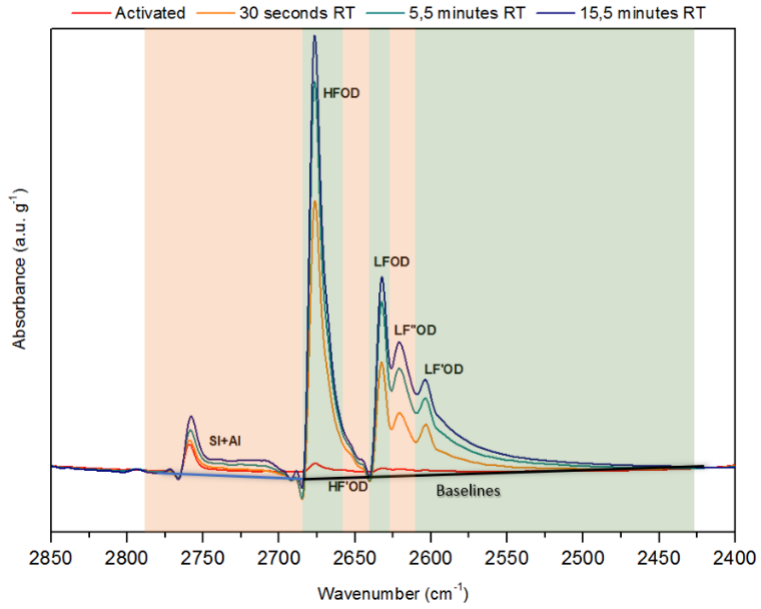

Figure 28: Direct integration on the deuteroxyl region of CBV720

C - Molar extinction coefficient for zeolites

The strategy used to calculate the molar extinction coefficients will be henceforth explained. As the quantification of the acid sites was obtained by direct integration of the FSD treated spectra, the first step was to determine the correction factor when using these treated spectra opposed to the original spectra.

After finding the correction factor, the molar extinction coefficient was calculated according to the literature [35]. The used HFOH molar extinction coefficient had a value of 2,9 cm μmol^{-1} [35]. The expressions used to calculate the extinction coefficient for LFOH, HFOD and LFOD are given by equations *(C.1)*, *(C.2)* and *(C.3)*, respectively.

$$\varepsilon_{LFOH} = (1 + 0{,}018\Delta\nu_{OH})\varepsilon_{HFOH} \qquad (C.1)$$

$$\varepsilon_{HFOD} = C\varepsilon_{HFOH} \qquad (C.2)$$

$$\varepsilon_{LFOD} = (1 + \frac{0{,}018\Delta\nu_{OH}}{0{,}737})\varepsilon_{HFOD} \qquad (C.3)$$

In these expressions, $\Delta\nu_{OH}$ is the wavenumber shift between the bands in the hydroxyl region and in the deuteroxyl region, and C is a correlation factor that depends on the family of the zeolite, with a value of 0,737 [35] being used (values comprised between 0,63 and 0,78 for faujasite type zeolites). Table 9 summarizes the results obtained for the molar extinction coefficients of each zeolite sample.

Table 9 : Molar extinction coefficients for all zeolites under study

	Wavenumber (cm^{-1})			Extinction coefficient ε (cm μmol^{-1})			
Sample	**HFOH**	**LFOH**	**Δv (OH)**	ε_{HFOH}	ε_{LFOH}	ε_{HFOD}	ε_{LFOD}
CBV500	3626	3550	75		9,1		6,7
Calcined CBV500	3627	3559	68		8,6		6,3
CBV712	3630	3565	65		8,4		6,1
Calcined CBV712	3629	3565	65		8,4		6,1
CBV720	3629	3565	64	3,2	8,3	2,4	6,1
CBV720 2nd batch	3628	3565	63		8,3		6,1
Steamed CBV720	3630	3566	64		8,3		6,1
Modified CBV720	3631	3565	66		8,5		6,2
CBV760	3630	3565	65		8,4		6,1

Having these values, the concentration of adsorbing species, n (μmol g^{-1}), can be calculated from the absorbance, d (a.u g^{-1}), by employing the Beer Lambert law (2.2.4).

$$d = \varepsilon_\nu \left(\frac{n}{S}\right) \qquad (C.4)$$

D - Quantification of the acid sites in zeolites

Table 10 : Direct Integration results of all the zeolitic samples under study for the activated spectra and after 15 minutes contact with C_6D_6 for both the hydroxyl and the deuteroxyl region (n.a. – not available)

	Sample / Acid Site	**CBV500**	**Calcined CBV500**	**CBV712**	**Calcined CBV712**	**CBV720**	**CBV720 2nd batch**	**Steamed CBV720**	**Modified CBV720**	**CBV760**
Activated Spectra (Hydroxyl Region)	**LF'**	n.a	n.a	119	228	200	210	n.a	n.a	n.a
	LF''	n.a	n.a	85	191	169	175	n.a	n.a	169
	LF	2411	1386	164	176	152	134	62	421	142
	HF'	1064	766	186	113	97	77	n.a	n.a	42
	HF	752	502	262	363	348	302	93	235	313
	Si+Al	692	567	381	1165	886	1152	605	2101	1568
15 minutes contact with C_6D_6 (Hydroxyl Region)	**LF'**	n.a	n.a	52	78	33	72	n.a	n.a	n.a
	LF''	n.a	n.a	40	56	29	53	n.a	n.a	41
	LF	670	912	83	47	27	40	10	377	16
	HF'	536	573	131	67	48	40	n.a	n.a	23
	HF	213	286	106	34	60	33	26	164	29
	Si+Al	460	516	354	1199	798	1151	586	2104	1532
15 minutes contact with C_6D_6 (Deuteroxyl Region)	**LF'**	n.a	n.a	114	175	152	168	35	57	183
	LF''	877	209	43	90	97	86	13	11	61
	LF	414	117	45	107	107	82	19	41	134
	HF'	241	125	48	36	36	40	33	19	68
	HF	363	171	162	274	221	228	41	70	236
	Si+Al	173	47	47	61	121	77	45	44	187